Tracking Agulhas leakage in the South Atlantic using modern planktic foraminifera nitrogen isotopes

Robyn Granger[1], Sandi Smart[2], Alan Foreman[3], Alexandra Auderset[3], Ethan Chen Campbell[4], Tanya A. Marshall[1], Gerald Haug[5], Daniel M. Sigman[6], Alfredo Martinez-Garcia[3], and Sarah E. Fawcett[1]

[1]University of Cape Town
[2]The University of Alabama
[3]Max Planck Institute for Chemistry
[4]University of Washington
[5]ETH Zurich
[6]Princeton University

April 02, 2024

Tracking Agulhas leakage in the South Atlantic using modern planktic foraminifera nitrogen isotopes

R. Granger[1,2]*, S.M. Smart[1,3], A. Foreman[2], A. Auderset[2,4], E.C. Campbell[5†], T.A. Marshall[1,5], G.H. Haug[2], D.M. Sigman[5], A. Martínez-García[2], S.E. Fawcett[1,6]

[1] Department of Oceanography, University of Cape Town

[2] Climate Geochemistry Department, Max Planck Institute for Chemistry

[3] Department of Geological Sciences, The University of Alabama

[4] School of Ocean and Earth Science, University of Southampton

[5] Department of Geosciences, Princeton University

[6] Marine and Antarctic centre for Research and Innovation and Sustainability (MARIS), University of Cape Town

[*] now at NIOZ Royal Netherlands Institute for Sea Research, Department of Marine Microbiology and Biogeochemistry

[†] Now at School of Oceanography, University of Washington, Seattle, WA, USA

Corresponding authors: Robyn Granger (robyn.granger@nioz.nl); Sarah Fawcett (sarah.fawcett@uct.ac.za)

Key Points:

- Nitrogen isotope ratios of mixed-layer nitrate, zooplankton, and foraminifera in an Agulhas eddy are low compared to Cape Basin waters.
- Deep-dwelling foraminifera record the N isotope ratio of thermocline nitrate, which is lower in Agulhas waters than in the South Atlantic.
- Foraminifer-bound nitrogen isotopes in the Cape Basin sediment record could be used to reconstruct past variations in Agulhas leakage.

Abstract

Seawater transported into the South Atlantic from the Indian Ocean via "Agulhas leakage" modulates global ocean circulation and has been linked to glacial-interglacial climate cycles. However, constraining past Agulhas leakage remains a challenge. Using new measurements from the modern South Atlantic, we propose that the $\delta^{15}N$ of organic matter preserved in the shells of fossil planktic foraminifera could be used to infer past changes in Agulhas leakage. We sampled a transect of the Cape Basin in winter 2017 that intersected a mature Agulhas eddy and found that mixed-layer nitrate-, zooplankton-, and foraminifer-$\delta^{15}N$ (tissue and shells) was 2-3‰ lower in the eddy than the background Atlantic even though the $\delta^{15}N$ of the underlying thermocline nitrate was indistinguishable. We suggest that the $\delta^{15}N$ of eddy-N reflects Agulhas Current thermocline nitrate, which is ~2‰ lower than that of the South Atlantic due to N_2 fixation that occurs in the Indian Ocean. Foraminifera $\delta^{15}N$ may have been further lowered during eddy migration by *in-situ* N_2 fixation and/or recycling of low-$\delta^{15}N$ ammonium. The absence of low-$\delta^{15}N$ Agulhas nitrate in the eddy thermocline can be explained by convective mixing of thermocline and mixed-layer waters at the Agulhas Current Retroflection where eddies form, and the subsequent consumption of Agulhas nitrate by phytoplankton in the mixed layer, which raises its $\delta^{15}N$. The low $\delta^{15}N$ of eddy foraminifera, apparent even after several months of eddy migration across the Cape Basin, suggests that fossil foraminifer-bound $\delta^{15}N$ from the region may record variations in past Agulhas leakage.

Plain Language Summary

"Agulhas leakage", the flow of seawater from the Indian to the Atlantic Ocean, is a key component of global ocean circulation and predominantly takes the form of eddies. Identifying past changes in leakage can provide insights into the relationship between Atlantic Ocean circulation and climate changes. Here, we suggest that the nitrogen isotopes of organic matter preserved in the shells of fossil foraminifera, single-celled zooplankton, could be used to investigate past Agulhas leakage. Thermocline nitrate has a lower nitrogen isotope ratio in the Agulhas Current region than in the South Atlantic; to determine whether foraminifera inhabiting Agulhas leakage reflect this trend, we collected living specimens from inside and outside of a well-developed Agulhas eddy in the southeastern Atlantic. We found the nitrogen in foraminifera biomass and shells to be isotopically lower in the eddy than in the "background" southeastern Atlantic. This signal can be explained by the lower nitrogen isotope ratio of the original (Agulhas-sourced) nitrate, potentially augmented by internal nitrogen cycle processes that occurred during eddy migration, including dinitrogen fixation and ammonium recycling. Our results strongly suggest that the nitrogen isotopes of fossil foraminifera could be used as an indicator of past variations in Agulhas leakage.

1 Introduction

The southeast Atlantic Ocean is important for global ocean-atmosphere dynamics because it is the site of heat and salt transport from the Indian to the Atlantic Ocean, a process that is fundamental to the Atlantic Meridional Overturning Circulation (AMOC) (Fig. 1; Gordon, 1986; De Ruijter et al., 1999; Garzoli and Matano, 2011; Rühs et al., 2013). Warm, saline upper Indian Ocean waters enter the South Atlantic via large anticyclonic eddies, jets, and filaments that flow into the Cape

Basin (Duncombe Rae, 1991; Ballegooyen et al., 1994; Schouten et al., 2000); this "Agulhas leakage" is the only pathway by which Indian Ocean waters enter the Atlantic (Gordon, 1986; De Ruijter et al., 1999; Beal et al., 2011; Rühs et al., 2013). The spawning of Agulhas eddies occurs at the Agulhas Retroflection where the Agulhas Current loops anticyclonically back on itself to form the eastward-flowing Agulhas Return Current (Gordon et al., 1987; Lutjeharms and Valentine, 1984; De Ruijter et al., 1999; Beal et al., 2011). Some Agulhas water escapes at the Retroflection to form mesoscale anticyclonic eddies (the largest of which are termed "Agulhas rings"; Lutjeharms and Gordon, 1987), which then either dissipate in the Cape Basin or continue past the Walvis Ridge into the southwest Atlantic, occasionally even entering the North Atlantic (Goni et al., 1997; Arhan et al., 1999; Schouten et al., 2000).

Once in the Cape Basin, Agulhas eddies rapidly lose the warm temperatures of their (sub)tropical Indian Ocean source waters (Goni et al., 1997; Olson et al., 1992; Schouten et al., 2000; Schmid et al., 2003). They can nonetheless be identified by a characteristic positive sea-surface height anomaly (SSHA) associated with convergence at their centres, as well as elevated salinity, which persists on advective timescales (Gordon and Huber, 1990; Ballegooyen et al., 1994; Schouten et al., 2000). The export of relatively saline waters from the Indian Ocean by Agulhas eddies contributes to the densification and subduction of surface waters in the North Atlantic (through the formation of North Atlantic Deep Water (NADW); Gordon et al., 1992; Donners et al., 2005; Garzoli and Matano, 2011), which leads to freshly oxygenated deep waters spreading southwards via the AMOC's lower limb (Gordon, 1986; Rintoul 1991; Wefer et al., 1996; Garzoli and Matano, 2011; Ferreira and Kerr 2017). It has been suggested that decreased Indo-Atlantic exchange during ice ages inhibited NADW production, weakening the AMOC, while a deglacial increase in Agulhas leakage may have helped to re-establish warmer interglacial conditions by strengthening the AMOC (Berger and Wefer, 2002; Weijer et al., 2002; Knorr and Lohmann, 2003; Peeters et al., 2004). Long-term variability in Agulhas leakage thus has global-scale climate implications (Schouten et al., 2000; Van Aken et al., 2003; Beal et al., 2011).

Past variations in Agulhas leakage have been reconstructed from the species composition of planktic foraminifera, single-celled zooplankton with calcite shells that can be preserved in seafloor sediments for millions of years (Bé and Hutson, 1977; Schiebel and Hemleben, 2005). This approach employs the sedimentary ratio of (sub)tropical Indian Ocean species (termed "Agulhas leakage fauna") to species better adapted to cooler South Atlantic conditions as an indicator of the strength of leakage (Peeters et al., 2004; Lončarić, 2006; Caley et al., 2014). The idea is that foraminifera originating in (sub)tropical Indian Ocean waters are transported via Agulhas eddies into the South Atlantic where they sink and accumulate on the seafloor. The stronger the Agulhas leakage, the more abundant the (sub)tropical foraminifera in the sediments relative to the temperate Atlantic species (Peeters et al., 2004; Martínez-Méndez et al., 2010; Caley et al., 2011, 2012).

Attempts to ground-truth this assemblage-based approach using modern foraminifera indicate that it works well for young Agulhas eddies (< 9 months old) located near the Retroflection (Peeters et al., 2004; Caley et al., 2014). However, foraminifer species collected from a mature Agulhas eddy (> 10 months old) in the Cape Basin were found to be indistinguishable from the species sampled in South Atlantic waters surrounding the eddy (Lončarić, 2006). The implication of this finding is that although conditions within an Agulhas eddy may initially favour (sub)tropical foraminifera,

changes in the eddy environment with time (e.g., rapid heat loss; Ballegooyen et al., 1994) prevent their sustained growth, allowing them to be succeeded by temperate Atlantic species (Lončarić, 2006). This pattern of succession will ultimately be communicated to the sediment record, with temperate foraminifera potentially overwhelming the Agulhas assemblage and, by extension, the evidence of leakage. There is thus a need for alternative proxies that better preserve the signal of Agulhas leakage, especially beyond the region of eddy formation.

As previous unpublished work has hypothesized (Campbell, 2016), a potential candidate proxy for tracking Agulhas leakage is the nitrogen (N) isotopic composition of organic matter encased within the calcite tests of planktic foraminifera (i.e., foraminifer-bound $\delta^{15}N$, where $\delta^{15}N$ (in ‰ *versus* N_2 in air) = $[(^{15}N/^{14}N)_{sample}/(^{15}N/^{14}N)_{air} - 1] \times 1000$). This organic matter appears less vulnerable to diagenetic change and/or contamination than bulk particulate organic N (PON) that sinks from the surface layer to accumulate on the seafloor (Altabet and Francois, 1994; Meckler et al., 2011; Holmes et al., 2002; Robinson et al., 2012). During chamber formation, foraminifera precipitate calcite onto an organic sheet containing N-rich amino acids (Bé et al., 1977 King and Hare, 1972; Hemleben et al., 1977; Spero, 1988). This material ends up encased within the foraminifer calcite matrix (Bé et al., 1979; Hemleben et al., 1985) where its composition appears largely protected from alteration (Martínez-García et al., 2022), including during sinking and burial in the sediments (King and Hare, 1972; Robbins and Brew, 1990; Ren et al., 2009, 2012; Smart et al., 2018) where it can be preserved for millions of years (Kast et al., 2019; Auderset et al., 2022, Moretti et al., 2024).

An assumption inherent to applications of foraminifer-bound $\delta^{15}N$ to sediment records is that the $\delta^{15}N$ of the organic N encased within a foraminifer shell is a good indicator of foraminifer ecology and/or the environmental conditions experienced during the organism's lifetime (which can range from weeks to a year, depending on the species; Bé et al., 1979). Recent comparisons of the $\delta^{15}N$ of foraminifer tissue (FT-$\delta^{15}N$) and shells have revealed a near 1:1 relationship and relatively consistent offset (of ~1‰) between the two in the mixed layer (Ren et al., 2012; Smart et al., 2018, 2020). Additionally, foraminifer-bound $\delta^{15}N$ appears to change only slightly between the mixed layer and twilight zone, and then remains constant until foraminifera are incorporated into the sediments (Smart et al., 2018). In low-latitude regions where surface-water nitrate is always low, there is a strong link between foraminifer-bound $\delta^{15}N$ and the $\delta^{15}N$ of thermocline nitrate supplied to the surface annually (Ren et al., 2009, 2012; Smart et al., 2018). By contrast, in the high-latitudes where phytoplankton do not fully consume surface nitrate, foraminifer-bound $\delta^{15}N$ is expected to reflect the extent of nitrate drawdown (Martínez-García et al., 2014; Ren et al., 2015). This is because isotope fractionation during nitrate assimilation causes the $\delta^{15}N$ of nitrate (and phytoplankton biomass, part of the foraminifer's diet) to rise as the nitrate concentration declines (Altabet and Francois, 1994; Sigman et al., 1999); as such, more complete nitrate consumption should increase foraminifer-bound $\delta^{15}N$. However, a recent ground-truthing study from the Southern Ocean showed that on a seasonal basis, the modern FT-$\delta^{15}N$ (i.e., the non-calcified biomass of living foraminifera) is more strongly linked to the $\delta^{15}N$ of PON than to the $\delta^{15}N$ of nitrate (Smart et al., 2020). In addition, because the lifespan of most species is much shorter than a year, foraminifer-bound $\delta^{15}N$ and FT-$\delta^{15}N$ can also reflect changes in upper ocean N cycling (Smart et al., 2018, 2020). Thus, accurately interpreting variations in fossil foraminifer-bound $\delta^{15}N$ may thus require some knowledge of foraminifer ecology at the species level.

On an annual basis, the $\delta^{15}N$ of symbiont-bearing foraminifera (shells and tissue) in the low-latitude ocean (Sargasso and South China Seas) has been shown to record the $\delta^{15}N$ of shallow thermocline nitrate almost without offset, while the $\delta^{15}N$ of foraminifera without symbionts is generally 1–2‰ higher than that of the source nitrate (Ren et al., 2009, 2012; Smart et al., 2018). Given the demonstrated sensitivity of low-latitude foraminifer $\delta^{15}N$ to thermocline nitrate (Ren et al., 2009, 2012; Schiebel et al., 2018), we propose that foraminifer-bound $\delta^{15}N$ provides a potential proxy for monitoring Agulhas leakage into the South Atlantic. While both the South Atlantic and Indian Oceans rely on Subantarctic Mode Water (SAMW) as the ultimate source of their mixed-layer nitrate (Sarmiento et al., 2004; Palter et al., 2010), the $\delta^{15}N$ of nitrate in the subtropical Indian thermocline is substantially lower than that observed in the subtropical South Atlantic (<5.4‰ *versus* ~6.8‰; Marshall et al. 2023; Flynn et al. 2020; Marconi et al. 2017). This difference is likely due to the occurrence of N_2 fixation in the southwest Indian Ocean but not in the subtropical South Atlantic (Moore et al., 2009; Harms et al., 2019; Marshall et al., 2023). N_2 fixation introduces bioavailable N to the upper water column that is low in $\delta^{15}N$ (-2 – 0‰; Carpenter et al., 1997; Hoering and Ford, 1960; Minagawa and Wada, 1986), ultimately causing the $\delta^{15}N$ of thermocline nitrate to decline relative to the underlying source waters (Knapp et al. 2008). In other ocean regions that host significant rates of N_2 fixation, such as the (sub)tropical North Atlantic, the low $\delta^{15}N$ of thermocline nitrate is passed on to phytoplankton (Fawcett et al., 2011, 2014; Van Oostende et al., 2017) and zooplankton (Somes et al., 2010; Loick-Wilde et al., 2016), including foraminifera (Ren et al., 2012; Smart et al., 2018). We thus expect the PON produced from the consumption of Agulhas nitrate (including Agulhas eddies), as well as the foraminifera reliant thereon, to be lower in $\delta^{15}N$ than those from the Cape Basin. For a $\delta^{15}N$-based leakage proxy to add value beyond existing proxies, a distinct $\delta^{15}N$ signature must persist in foraminifer-bound N regardless of changes in the eddy foraminifer assemblage.

Here, we investigate the potential utility of foraminifer-bound $\delta^{15}N$ as a proxy for Agulhas leakage and lay the groundwork for its application to palaeoceanographic records from the Cape Basin. We present measurements of nitrate isotope ratios for samples collected in 2015 and 2017 along a transect extending from the west coast of South Africa, across the Cape Basin, and into the South Atlantic subtropical gyre that intersected Agulhas eddies. For the 2017 sampling, we also measured the $\delta^{15}N$ of various forms of PON and of the tissue and shells of living planktic foraminifera captured in shallow net tows, both within an Agulhas eddy and in the "background" (i.e., non-eddy) South Atlantic. We compare our data to new nitrate isotope measurements from the Agulhas Current (Marshall et al., 2023) and confirm that Agulhas thermocline nitrate is low in $\delta^{15}N$ compared to the $\delta^{15}N$ of nitrate in SAMW and the Cape Basin thermocline. Our results show that foraminifera living in Agulhas eddies have a unique and persistent $\delta^{15}N$ signature, which we propose could be leveraged to reconstruct past Agulhas leakage.

2 Materials and Methods

2.1 Shipboard sampling

The South Atlantic Meridional Overturning Circulation Basin-wide Array (SAMBA) is a zonal transect of moorings along 34.5°S (Morris et al., 2017). In 2017, we sampled 21 conductivity-temperature-depth (CTD) hydrocast stations the eastern sub-array of SAMBA (i.e., east of 0°E)

for a variety of physical, chemical, and biological parameters (Fig. 1). We supplemented this dataset with hydrographic, nutrient, and nitrate isotope measurements from five hydrocasts conducted along the same array in 2015 (Campbell et al., 2016; Marconi et al., 2017; C1-C5 in Fig. 1). In both years, sampling occurred during austral winter (July) aboard the R/V *S.A. Agulhas II*, with water-column samples collected using Niskin bottles attached to a rosette equipped with Sea-Bird CTD, oxygen, and fluorescence sensors that assisted in targeting specific features (e.g., the mixed layer depth (MLD) and depth of maximum fluorescence (F-max)). In 2017, the cruise detoured south (to 35.5°S) between 11.2°E and 14.3°E to sample an anticyclonic Agulhas eddy (hereafter referred to as E1) that was tracked prior to and during the cruise using satellite altimetry (see section 2.4).

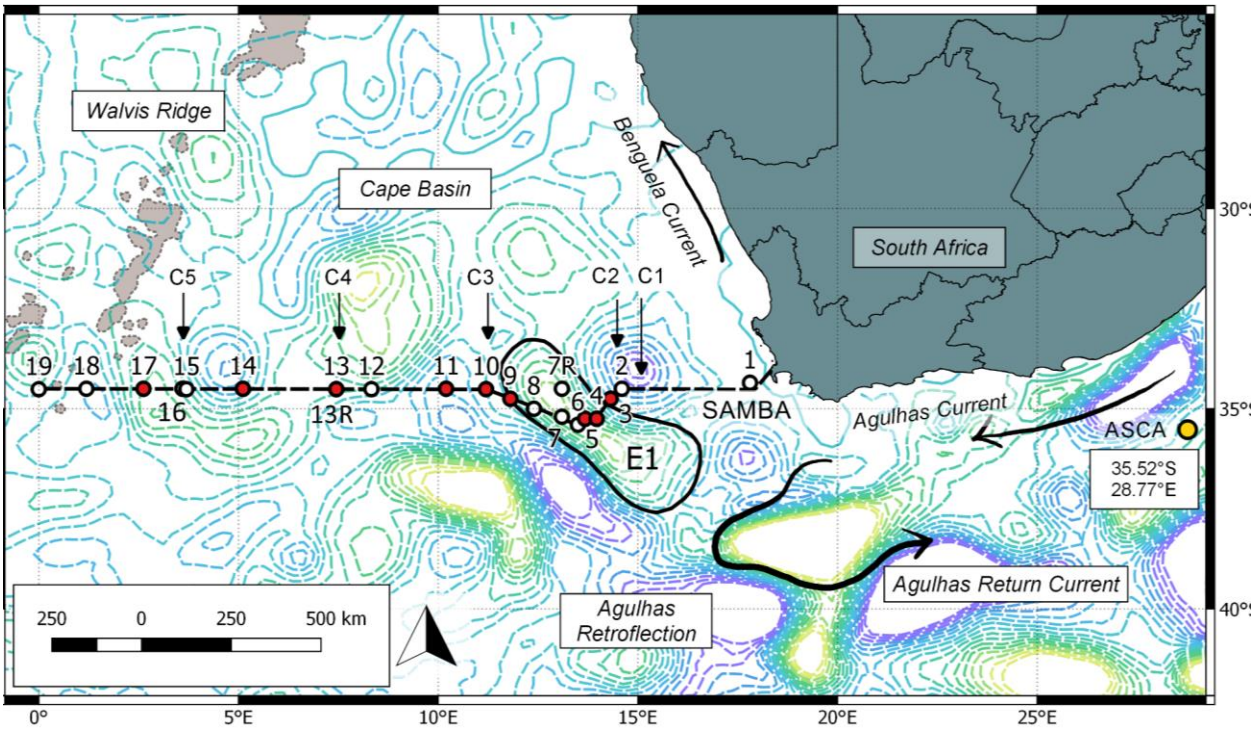

Figure 1. Cruise track followed by the R/V *S.A. Agulhas II* in July 2017 along the SAMBA line. Contour lines show sea surface height anomaly (SSHA) relative to the geoid (SSALTO/DUACS product distributed by AVISO via the Copernicus Marine Environment Monitoring Service (Lea et al., 2018); http://marine.copernicus.eu, 24 July 2017), with positive and negative anomalies shown by the light green and purple dashed lines, respectively. The outer edge of Agulhas eddy E1, as defined in section 2.4, is indicated by the thick black contour. Along the transect, the white circles represent stations sampled for nitrate concentration, isotopes, and particulate organic nitrogen while red circles show stations where foraminifera and bulk zooplankton were additionally collected using net tows. The positions of stations sampled in 2015 along the same 34.5°S transect (Campbell et al., 2016; Marconi et al., 2017) are indicated by arrows and labelled C1-C5, noting that the background SSHA does not apply to these stations. The position of a station located in the Agulhas Current region in the southwest Indian Ocean that was sampled in July 2016 is indicated by the yellow circle.

In July 2016, samples were collected for nitrate concentrations and isotopes aboard the R/V *S.A. Agulhas II* along the Agulhas System Climate Array (ASCA) transect in the southwest Indian Ocean that extends 300 km offshore of South Africa across the Agulhas Current (Morris et al., 2017; Marshall et al., 2023). From these samples, a representative station (35.52°S; 28.77°E) located just offshore of the current core was selected for comparison with the SAMBA stations (yellow circle in Fig. 1). Samples were processed as described for the SAMBA collections, with measurements from the entire ASCA transect detailed in Marshall et al. (2023).

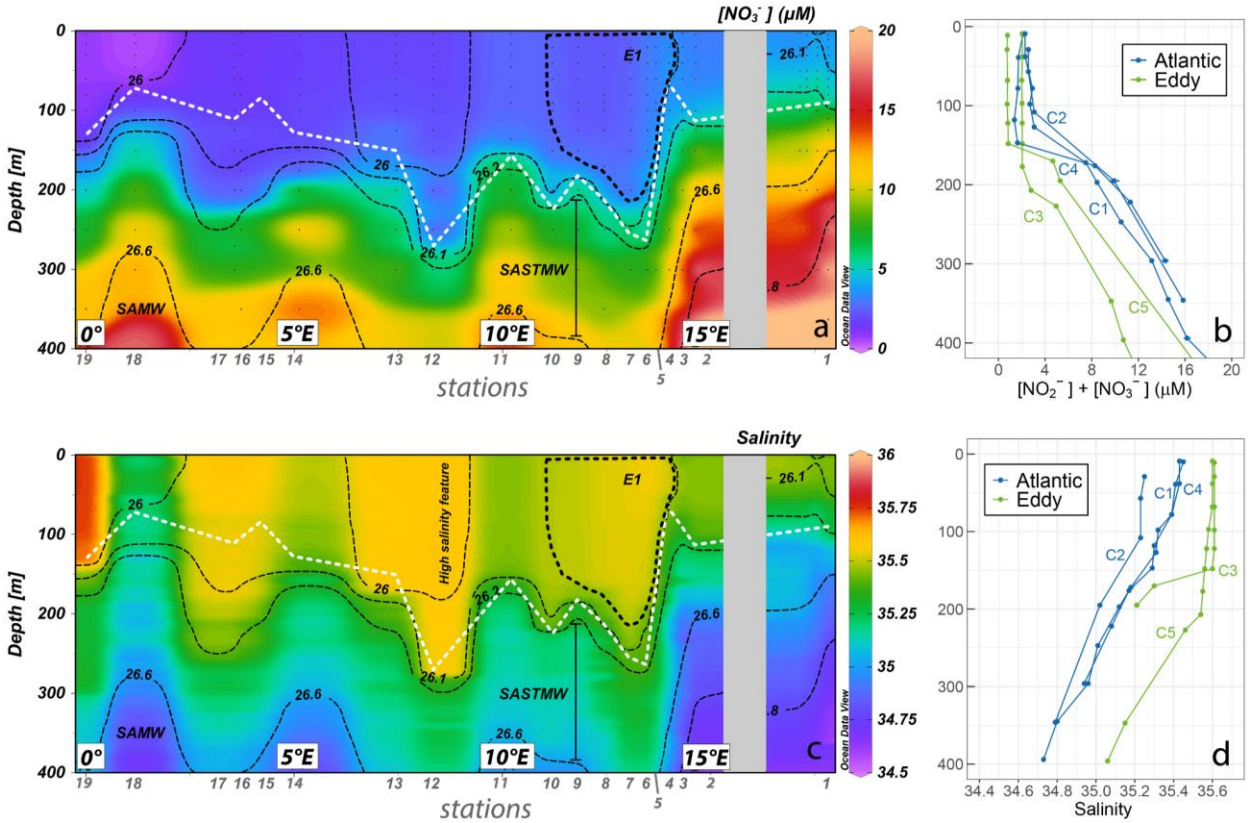

Figure 2. Section plots from the 2017 cruise showing a) nitrate concentration and c) salinity overlaid with isopycnals (kg.m^{-3}; dotted black contour lines). Subantarctic Mode Water (SAMW) and South Atlantic Subtropical Mode Water (SASTMW) are defined by density. The approximate mixed layer depth is indicated by the dashed white line. Sampling stations are labelled on the bottom x-axis, and the location of Agulhas eddy E1 is shown by the dashed black polygon (labelled E1). Panels b) and d) show the vertical profiles of nitrate and salinity for the stations sampled in 2015, with the colours indicating whether those stations were located in background Atlantic- (blue) or Agulhas eddy waters (green) at the time of sampling.

For both the 2015 and 2017 SAMBA datasets, MLD was calculated as the depth at which potential density exceeded the value at 25 m by 0.05 kg.m^{-3}. These derived MLDs closely tracked the 26.1 – 26.2 kg.m^{-3} isopycnals that denote the top of the thermocline and yielded upper layers over which the nitrate concentrations were near-homogeneous (Fig. 2a, 2b).

All CTD stations were sampled for seawater nitrate+nitrite and nitrite concentrations, with five and 19 stations also sampled for nitrate isotopes in 2015 and 2017, respectively. Seawater was collected in well-rinsed 50 mL polypropylene tubes for nutrients and high-density polyethylene bottles for nitrate isotopes, with the latter immediately frozen at -20°C. The nitrate+nitrite concentrations were measured shipboard using a Lachat QuickChem flow injection autoanalysis platform (Grasshoff, 1976; Diamond, 1994) in a configuration with a detection limit of 0.1 μM. Nitrite concentrations were determined manually via the colorimetric method of Strickland and Parsons (1968) using a Thermo Scientific Genesys 30 visible spectrometer. Certified reference materials (KANSO; lots CG, CH, and CE) were included in each nitrate+nitrite and nitrite run to ensure measurement accuracy. Nitrate-only concentrations were calculated by subtraction.

In 2017, four to six bulk suspended PON samples were collected over the mixed layer (0 – 175 m) at all stations. We targeted the surface (< 10 m), the F-max, and two to four additional depths including the approximate MLD. At each depth, 4 L of seawater were filtered through pre-combusted (450°C for 8 hours) 0.3 μm glass fibre filters (GF-75; Sterlitech) that were then stored frozen in pre-combusted foil at -80°C until processing.

Living planktic foraminifera were collected at nine stations (Fig. 1, red circles) using a double 1 m^2 250 μm-mesh plankton net, towed obliquely over the upper 200 m at 0.1-0.6 knots for ~40 minutes. On deck, around 90% of each collection was preserved using 5-10% pH-buffered formalin and refrigerated at 4°C until processing, following the protocol of Smart et al. (2020) (modified from Ren et al., 2012). The remaining 10% was size-fractionated on board for later analysis of bulk zooplankton $\delta^{15}N$ by sieving the material in series through nylon mesh sieves of 5000 μm, 2000 μm, 1000 μm, 500 μm, 250 μm, and 150 μm. The contents of each sieve were transferred to pre-combusted 0.7 μm glass fibre filters (GF/Fs; Whatman) and frozen at -20°C until processing.

2.2 Foraminifera and bulk zooplankton sample preparation

Sample preparation took place in the Marine Biogeochemistry Lab at the University of Cape Town (UCT-MBL), South Africa, and the Max Planck Institute for Chemistry (MPIC) in Mainz, Germany. Foraminifera were picked according to the methods outlined in Ren et al. (2012) and Smart et al. (2020). Briefly, formalin-preserved material was passed through a 1000 μm-mesh sieve to remove large zooplankton, then rinsed several times with deionized water. A density separation was subsequently performed using a 200 $g.L^{-1}$ NaCl solution before the foraminifer-containing material was rinsed again with deionized water and transferred to clean plastic petri dishes, and the liquid was allowed to evaporate under a fume hood.

For tissue measurements, between three and 14 specimens of each species were picked, photographed (Olympus UC90 camera), and transferred to weighed, pre-combusted (500°C for 5 hours) 4 mL Wheaton vials. Picked foraminifera were rinsed with Milli-Q water under an Olympus incident light microscope using a pipette to remove residual nitrate and formalin (Ren et al., 2012; Smart et al., 2020), then the remaining liquid was removed, and the samples were dried in a desiccator overnight. Specimens were weighed (Mettler Toledo XP6U comparator 7-digit microbalance), crushed inside the vial with an ethanol-cleaned spatula, and transferred to a -20ºC

freezer until oxidation. Shell samples were treated in the same way, but using between 15 and 100 specimens per vial.

Persulfate oxidising reagent (POR; 1 mL) was added to each tissue (1 g of four-times recrystallized potassium persulfate combined with 0.7 g NaOH and dissolved in 100 mL Milli-Q water) or shell sample (1.5 g potassium persulfate and 1.5 g NaOH dissolved in 100 mL Milli-Q water) to convert the external (tissue) organic N to nitrate, facilitated by autoclaving for 65 minutes at 120°C on a slow vent setting (Nydahl, 1978; Knapp et al., 2005). Samples were prepared in triplicate in different oxidation batches (with the exception of rare species). POR blanks and a dilution series of the amino acid standards, USGS-40 and USGS-41 (Qi et al., 2003), were included in all batches and used to quantify the magnitude and $\delta^{15}N$ of the POR-associated N blank and ensure complete oxidation (standards). After autoclaving, tissue samples were pH-adjusted to 5-7 using 4 N Optima grade HCl. For shell samples, the tissue-derived nitrate was removed, the samples were rinsed 4 times with Milli-Q water, and the remaining calcite was left to dry overnight at 40°C (Ren et al., 2009). Samples were then transferred to clean Wheaton vials to which 50 µL of 4 N HCl was added to release the calcite-bound organic N into solution. This biomineral-derived organic N was oxidized to nitrate via the addition of POR (in this case, 0.7 g of potassium persulfate and 4 mL of 6.25 M NaOH in 96 mL Milli-Q), after which sample pH was adjusted to 5-7.

Size-fractionated zooplankton samples were prepared for N isotope analysis by freeze-drying at -80°C using a Scanvac Coolsafe. Where possible, the dried material was gently scraped from the GF/F into a tin cup and weighed. Between 0.125 and 0.750 mg of sample was analysed. Where scraping was not possible due to small particles adhering to the GF/F, filter quarters were folded into tin cups and measured separately alongside blank pre-combusted filters. The bulk PON samples were prepared and analysed in the same way.

2.3 Particulate and nitrate isotope analysis

The concentration of nitrate resulting from the oxidation of foraminifer tissue and shells was measured by chemiluminescence (Braman and Hendrix, 1989; Ren et al., 2012). 10 nmol N (for tissue runs) or 5 nmol N (for shell runs) of nitrate was then quantitatively converted to N_2O gas via the denitrifier method (Sigman et al., 2001) and the $\delta^{15}N$ of the N_2O was measured by gas chromatography-isotope ratio mass spectrometry (GC-IRMS) at MPIC using a Thermo MAT253 with custom-built N_2O extraction and purification system (Weigand et al., 2016). N_2O isotope measurements were calibrated to N_2 in air using the nitrate reference materials, USGS-34 and IAEA-NO_3 (Gonfiantini et al., 1993; Böhlke et al., 2003). The pooled standard deviation (1 ∫) for USGS-34 was 0.09‰ (n = 71 samples, n = 7 runs) and 0.06‰ (n = 24, runs = 3) for tissue and shell runs, respectively. Pooled standard deviation for IAEA-NO_3 was 0.15‰ (n = 71 samples, n = 7 runs) and 0.01‰ (n = 23, runs = 3) for the tissue and shell runs. Amino acid standards USGS-40 and USGS-41 had pooled standard deviations of 0.05‰ and 0.15‰ (n = 5 runs), respectively, for tissue runs and 0.20‰ and 0.24‰ (n = 3 runs) for shell runs. The dilution series bracketed the range of foraminifer concentrations (5 - 50 nmol). Measurements from each batch run were corrected for the POR blank (which on average accounted for 0.7% of the N in the foraminifer tissue samples and 10.7% of the N in the shell samples). The pooled standard deviation for cleaning-and-oxidation replicates of the same sample (same species and tow) was 0.03‰ for the

tissue samples (n = 188). The N content of the shell samples was not high enough to run replicates. The average $\delta^{15}N$ of our blanks was -2.2 + - 3.2 ‰.

Seawater samples underwent nitrite removal via sulfamic acid addition (Granger and Sigman, 2009) prior to N and oxygen (O) isotope analysis since even very low concentrations of nitrite can significantly affect the measured $\delta^{15}N$ and $\delta^{18}O$ of nitrate+nitrite (where $\delta^{18}O$ (in ‰ *versus* Vienna Standard Mean Ocean Water (VSMOW)) = $[(^{18}O/^{16}O)_{sample}/(^{18}O/^{16}O)_{VSMOW} - 1] \cdot 1000$) (Casciotti and McIlvin, 2007; Fawcett et al., 2015; Smart et al., 2015). The $\delta^{15}N$ and $\delta^{18}O$ of nitrate ($\delta^{15}N_{NO3}$ and $\delta^{18}O_{NO3}$) were subsequently determined using the denitrifier-IRMS method (Sigman et al., 2001; Casciotti et al., 2002; Weigand et al., 2016). The pooled standard deviations for replicate measurements ($n \geq 2$) were 0.05‰ and 0.18‰ (n = 245) for $\delta^{15}N_{NO3}$ and $\delta^{18}O_{NO3}$, respectively.

The nitrate isotope data were used to calculate Δ(15-18), which equals $\delta^{15}N_{NO3} - \delta^{18}O_{NO3}$ (Sigman et al., 2005; Rafter et al., 2013). The ratio of the N and O isotope effects expressed during phytoplankton nitrate assimilation is approximately 1:1 (Granger et al., 2004, 2010), such that assimilation does not alter nitrate Δ(15-18). By contrast, processes that produce nitrate have disparate effects on its $\delta^{15}N_{NO3}$ and $\delta^{18}O_{NO3}$, and thus change Δ(15-18). This difference occurs because the $\delta^{15}N$ of nitrate produced by subsurface nitrification depends on the $\delta^{15}N$ of the organic matter and ammonium being remineralized and nitrified, while the $\delta^{18}O$ of newly-nitrified nitrate is set by the $\delta^{18}O$ of seawater (plus an isotopic offset of ~1.1‰; Sigman et al., 2005, 2009; Buchwald and Casciotti, 2010; Boshers et al., 2019)). As such, nitrate Δ(15-18) can be used to disentangle overlapping N cycle processes that cannot be diagnosed from measurements of $\delta^{15}N_{NO3}$ or $\delta^{18}O_{NO3}$ alone. For example, N_2 fixation introduces nitrate to the subsurface that is lower in $\delta^{15}N$ than deep-ocean nitrate, thus causing nitrate Δ(15-18) to decrease (e.g., Knapp et al. 2008; Marshall et al., 2023). Similarly, co-occurring partial nitrate assimilation and nitrification (e.g., at the base of the mixed layer), which has no net effect on $\delta^{15}N_{NO3}$ but causes $\delta^{18}O_{NO3}$ to rise (because the $\delta^{18}O$ of newly-nitrified nitrate is higher than the $\delta^{18}O$ of the nitrate removed by phytoplankton), yields a decline in nitrate Δ(15-18) (Sigman et al., 2005, 2009; Wankel et al., 2007; Rafter et al., 2013; Fawcett et al., 2015; Deman et al., 2021, Marshall et al., 2023).

The $\delta^{15}N$ of bulk PON and size-fractionated zooplankton were measured in the Stable Light Isotope Laboratory at UCT using a Delta V Plus IRMS coupled to a Flash 2000 elemental analyzer. In-house standards calibrated against IAEA reference materials were run after every 5-8 samples and used to reference the measurements to atmospheric N_2. The detection limit for N was 1 µg and precision was <0.2‰. On average, the filter blanks contributed 1.4% to the bulk zooplankton N concentration and 6.9% to the bulk PON samples. The pooled standard deviation for replicate sample analyses (n = 15) was 0.18‰.

2.4 Satellite imagery and model products

Satellite altimetry was used alongside ship-board hydrographic and acoustic Doppler current profiler (ADCP) data to track an Agulhas eddy before and during the SAMBA 2017 cruise. A large asymmetrical eddy (E1) formed in December 2016 and was evident at the time of sampling as a closed-contour, positive sea surface height anomaly (SSHA) > +7 cm (CMEMS, Fig. 1). E1 was characterized by high sea-surface salinity (> 35.5 $g.kg^{-1}$), depressed isopycnals (Fig. 2c), and anticyclonic rotation (apparent in the ADCP data; Wallschuss et al., 2022). For the 2015 cruise, Agulhas eddies were identified post-cruise from locally elevated water temperatures (by as much as 4.7°C at 250 m; Campbell, 2016), anticyclonic rotation (via ADCP), high mixed-layer salinity

(Fig. 2d), and the depression of isopycnals in the upper water column. Two additional eddies (E2, 7.5 – 8.3°E and E3, 3.6 – 3.7°E) were identified by Wallschuss et al. (2022) along the 2017 transect. Our stations 12, 13, 13R, 15, and 16 were located with these features (Fig. 1; where "R" indicates "repeat" since station 13 was sampled on both the outbound and inbound legs of the cruise). However, we classify only station 12 (8.3°E) as an eddy station and refer to stations 13, 13R, 15, and 16 as "mixed". This decision was based on (1) reduced rotation at the mixed stations due to their location at the eddy edges, and recognizing that the physical and biological properties at eddy edges can reflect either the eddy (e.g., station 3) or the background Atlantic (e.g., station 10); and (2) the low sampling resolution within E2 and E3, such that these features are not well defined (a limitation also noted by Wallschuss et al., 2022).

The CMEMS product, Global_Forecast_Bio_001_028, was used to visualize the seasonal cycle of surface (0.5 m) nitrate concentrations at four locations along 34.5°S over four years, encompassing the two cruises (2014 – 2018 at 0.25°E, 7.5°E, 10°E, and 13°E). This product uses the output from the PISCES model (Aumont et al., 2015), which simulates the daily cycles of carbon and nutrients. The surface nitrate concentration is resolved at 0.25° horizontal resolution.

3 Results

3.1 Hydrography and the identification of eddy stations

Eddy stations were distinguished from the background Atlantic using a combination of altimetry, density, and salinity data, along with the derived MLDs. Agulhas eddies are characterized by anticyclonic rotation, positive SSHAs, and deep, low-density, high-salinity mixed layers (Schouten et al., 2000; Van Aken et al., 2003; Moutin and Prieur, 2012; Dufois et al., 2016). In 2017, stations 4 to 9 were located within E1, with the stations on either side representing the eddy edges (Fig. 1 and 2). The most positive SSHA (+ 38 cm) was observed at station 7 (13.1°E), which we take to represent the core of E1. As expected, the E1 mixed layer was more saline than at the surrounding Atlantic stations (e.g., 35.55 $g.kg^{-1}$ at station 5 *versus* 35.45 $g.kg^{-1}$ at station 11; Fig. 2c).

Satellite imagery indicated the presence in 2017 of an additional eddy-like feature just north of our transect, with station 12 located at its southern edge (Fig. 1). The high-salinity, low-density, deep mixed layer (277 m; Fig. 2) at station 12 implicates Agulhas leakage, leading us to classify it as an eddy station. Agulhas leakage was less apparent at the neighbouring station 13 (and 13R). Here, the isopycnals shoaled rapidly, leading to shallower MLDs (158 m and 211 m). We classify these stations as mixed and as such, do not include them (or the E1 edge stations 3 and 10) in our comparisons of Atlantic and eddy seawater characteristics.

At the trailing (i.e., eastern) edge of E1, a dipole effect was evident, with the cyclonic circulation of a non-Agulhas eddy to the east creating a steep gradient in SSHA (approximately 50 cm over 100 km between stations 2 and 4; Fig. 1). The interaction of E1 with the cyclone altered the physical and chemical characteristics of the water column, evinced by a sudden shoaling of the mixed layer (to 67 m) and nitracline at stations 3 to 5 compared to the stations in the centre of E1 (Fig. 2b).

The average MLD in E1 was significantly greater than the average Atlantic MLD in 2017 (MLD = 216 ± 37 m (n = 5; stations 5 to 9) and 106 ± 40 m (n = 8; stations 2, 11, 14 to 19), respectively; Welch's t-test $p < 0.001$). Eddy station 4 was excluded from this analysis due to its much shallower mixed layer (67 m) resulting from isopycnal shoaling during the interaction of the trailing edge of E1 with the cyclone to its east. The same trend of deeper in-eddy mixed layers was evident in the 2015 dataset, with an average MLD of 187 ± 32 m (n = 2) for the eddy- (stations C3 and C5) and 139 ± 16 m (n = 3) for the Atlantic stations (C1, C2 and C4; Fig. 2b and 2d).

Using potential density, we identified several water masses in the upper 1000 m of the 2015 and 2017 transects. SAMW was evident between 26.6 and 27.0 $kg.m^{-3}$ (~350 to 750 m) and was overlaid by South Atlantic Subtropical Mode Water (SASTMW; 26.2 to 26.6 $kg.m^{-3}$; ~200 to 350 m), which is formed through the modification of SAMW by mixing with less dense surface waters (Donners et al., 2005). Surface waters overlying SASTMW had a potential density of 25.9 to 26.2 $kg.m^{-3}$, with the least dense waters encountered at the westernmost edge of the transect (i.e., station 19 in the subtropical gyre), as well as at mid-transect stations 12, 13, and 13R.

3.2 Seawater nitrate concentrations and isotopes

Mixed-layer nitrate concentrations were similar for the 2015 and 2017 transects (< 4.1 μM in 2017 and < 3.1 μM in 2015; Fig. 2a and 2b), with a consistent east-to-west decrease of ~0.2 μM per degree of longitude (Fig. S1). In E1, mixed-layer nitrate was on average 1.2 μM higher than in the background Atlantic. In 2015, the eddies were encountered further west along the transect, and eddy mixed-layer nitrate was on average 0.7 μM lower than in the Atlantic. Below the mixed layer, the nitrate concentration of SASTMW in 2017 was fairly uniform, averaging 8.6 ± 2.3 μM (n = 12) for the Atlantic stations and 8.5 ± 1.9 μM (n = 14) in E1; these concentrations are consistent with previous measurements of SASTMW in the southeast Atlantic (8.7 ± 2.6 μM; Flynn et al., 2020). The nitrate concentration of the underlying SAMW ranged from 11.3 to 23.6 μM (transect average of 16.7 ± 3.7 μM, n = 27), with no significant difference between the Atlantic stations and E1. The nitrate concentrations determined in 2015 for these water masses were similar; 9.2 ± 6.6 μM (n = 17) for SASTMW and 20.2 ± 5.6 μM (n = 13) for SAMW.

The surface (0.5 m) nitrate data from CMEMS agree well with our measured concentrations (Fig. 3). The model time-series shows that our sampling took place during the nitrate resupply period, which begins in late autumn (April/May). Surface nitrate concentrations peak in spring (September), reaching 4 to 5 μM at 13°E, 2 to 4 μM at 10°E, 1 to 3 μM at 7.5°E, and 1 to 2 μM at 0°E, and nitrate is almost completely exhausted by late summer (March/April). Comparing the nitrate concentration data from 2015 and 2017 with the model output suggests that both samplings captured typical winter conditions in the southeast Atlantic, and that the two years can be analysed as a single, combined dataset. Thus, unless otherwise stated, further discussion of water masses and seawater nitrate isotopes refers to a composite of the 2015 and 2017 datasets.

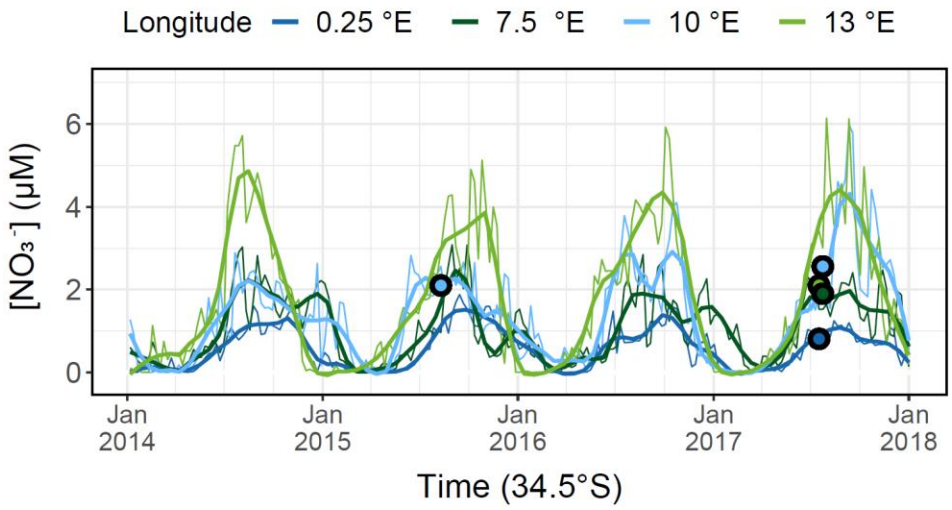

Figure 3. Surface (0.5 m) nitrate concentrations from the CMEMS product at four locations along the SAMBA transect (34.5°S; 0°E (dark blue), 7.5°E (dark green), 10°E (light blue), 13°E (light green)) between January 2014 and January 2018. The thin lines show monthly reanalysis data and the thick lines show smoothed data (moving average = 2 weeks) (http://marine.copernicus.eu/documents/QUID/CMEMS-GLO-QUID-001-028.pdf). Coloured circles show the surface nitrate concentrations measured at the corresponding locations during the 2015 and 2017 cruises.

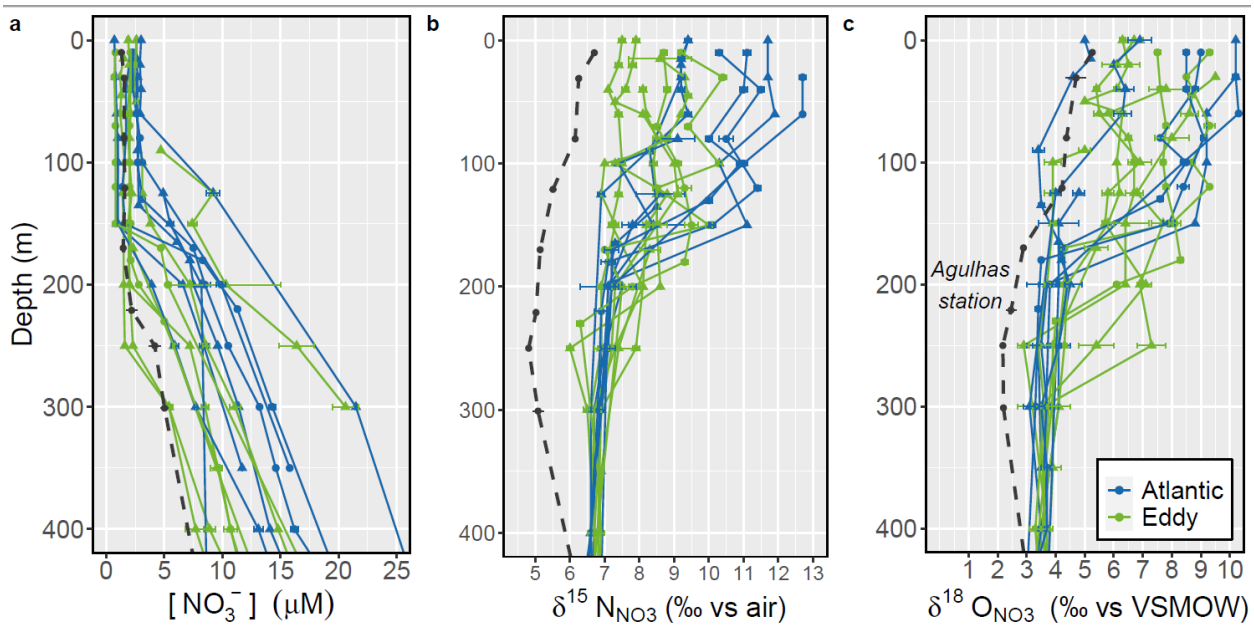

Figure 4. Depth profiles (0 – 400 m) of a) nitrate concentration, b) $\delta^{15}N_{NO3}$, and c) $\delta^{18}O_{NO3}$ for the SAMBA line stations sampled in 2015 and 2017, coloured by station type (blue = background Atlantic, green = Agulhas eddy). Triangles represent nitrate measurements

from 2015, whilst square symbols represent measurements from 2017. Also shown are data from a representative station located in the Agulhas Current region (dashed black line; Marshall et al., 2023). Error bars show ±1 standard deviation of duplicate measurements.

Across the transect, the mean $\delta^{15}N_{NO3}$ and $\delta^{18}O_{NO3}$ for SAMW was 6.5 ± 0.2 ‰ and 3.4 ± 0.4 ‰ (n = 58), respectively, while the mean SASTMW $\delta^{15}N_{NO3}$ was 6.9 ± 0.4‰ and $\delta^{18}O_{NO3}$ was 3.8 ± 0.6‰ (n = 51, Fig. 4). Above SASTMW, we observe a clear difference between eddy and Atlantic $\delta^{15}N_{NO3}$, but not $\delta^{18}O_{NO3}$ (Fig. 2.4b and c). While $\delta^{15}N_{NO3}$ increased from the thermocline (i.e., SASTMW) into the surface (< 20 m) at all stations, the magnitude of the increase was smaller at the eddy stations (average surface $\delta^{15}N_{NO3}$ of 8.6 ± 0.5‰ and 10.3 ± 0.8‰ for the eddy- (n = 19) and Atlantic stations (n = 40), respectively). Similarly, the concentration-weighted average mixed-layer $\delta^{15}N_{NO3}$ for the eddy stations (calculated using 1 m gridded values) was 7.9 ± 0.7‰ (i.e., 1.0‰ higher than mean SASTMW nitrate), while in the Atlantic mixed layer, $\delta^{15}N_{NO3}$ averaged 9.6 ± 1.2‰ (i.e., 2.7‰ higher than mean SASTMW nitrate). In addition, some of the E1 profiles showed a negative $\delta^{15}N_{NO3}$ deviation at the top of the thermocline (from 6.9‰ in SASTMW to as low as 6‰ at 230-250 m) that was not apparent at the Atlantic stations (nor in the $\delta^{18}O_{NO3}$ data). Like the $\delta^{15}N_{NO3}$, the $\delta^{18}O_{NO3}$ also increased from the thermocline into the mixed layer, but by similar amounts at the eddy- and Atlantic stations; averaged over the mixed layer, $\delta^{18}O_{NO3}$ was elevated relative to the thermocline by 2.3 ± 1.3‰ at the eddy stations and 2.8 ± 2.1‰ at the Atlantic stations.

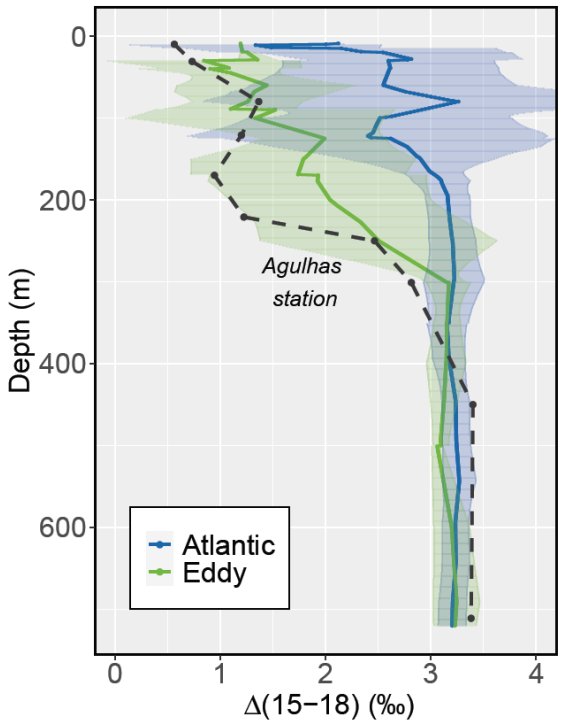

Figure 5. Average nitrate Δ(15-18) ($\delta^{15}N_{NO3} - \delta^{18}O_{NO3}$) at the Atlantic and eddy stations, gridded at 1 m intervals. Shaded areas indicate ±1 standard deviation of the combined 2015 and 2017 dataset. The black dashed line shows the nitrate Δ(15-18) for the Agulhas Current station included in Fig. 4 (Marshall et al., 2023).

The difference between the thermocline-to-mixed-layer changes in $\delta^{15}N_{NO3}$ and $\delta^{18}O_{NO3}$ in the eddy *versus* background Atlantic is highlighted by the nitrate Δ(15-18) profiles, where the influence of nitrate assimilation on $\delta^{15}N_{NO3}$ and $\delta^{18}O_{NO3}$ is effectively removed (Fig. 5; Rafter et al. 2013). Below the thermocline, all the seawater nitrate profiles converged on a Δ(15-18) of 3.2‰. At the eddy stations, Δ(15-18) then decreased through the thermocline and into the surface (average mixed-layer Δ(15-18) of 1.8 ± 1.2‰) whereas at the Atlantic stations, Δ(15-18) remained roughly constant between the thermocline and the surface (average mixed-layer Δ(15-18) of 3.0 ± 1.4‰).

At the Agulhas (i.e., ASCA) station, the mixed layer had a density of 25.4 $kg.m^{-3}$, which was low compared to the Cape Basin mixed layer, and a nitrate concentration of 1.2 ± 0.1μM, which was similar (Fig. 4a). While SAMW (26.6 – 27.0 $kg.m^{-3}$), with a core $\delta^{15}N_{NO3}$ and $\delta^{18}O_{NO3}$ of 6.9 ± 0.2‰ and 3.5 ± 0.2‰, respectively (Δ(15-18) of 3.4 ± 0.2‰; Marshall et al., 2023), also underlies the Agulhas Current thermocline, $\delta^{15}N_{NO3}$ decreased strongly into the thermocline (reaching a minimum of 4.9‰ at 250 m, Fig. 4b) and $\delta^{18}O_{NO3}$ decreased slightly (to a minimum of 2.2‰ at 250 m; Fig. 4c). The $\delta^{15}N_{NO3}$ and $\delta^{18}O_{NO3}$ subsequently increased into the mixed layer by 2.4‰ and 4.3‰, respectively (Fig. 5), similar to the increase observed in E1 (although offset to lower

values, particularly for $\delta^{15}N_{NO3}$). As such, mixed-layer $\delta^{15}N_{NO3}$ in the Agulhas profile (concentration-weighted average of 8.2 ± 0.8‰) was similar to that measured in the Cape Basin eddies and lower than in the Atlantic mixed layer (by 1.4‰), while its $\delta^{18}O_{NO3}$ (concentration-weighted mixed-layer average of 7.2‰) overlapped with the lower end of the mixed-layer values measured across the Cape Basin. The averaged mixed-layer Δ(15-18) for the Agulhas profile was 1.0 ± 0.3‰, which is 0.8‰ and 2.0‰ lower than at the eddy and Atlantic stations, respectively.

3.3 Foraminifera and particulate organic N isotopes

In our analysis of the foraminifera (tissue and shell) and particulate $\delta^{15}N$ data, we divide the stations into two groups, "eddy" and "Atlantic". We include the mid-transect "mixed" station 13 in the Atlantic group since, although it showed some properties consistent with an eddy-influenced environment (e.g., high salinity and positive SSHA), it was not enclosed by anticyclonic flow (Fig. 1). We also classify the leading edge of E1 (station 10) as Atlantic, as the upward-sloping isopycnals led to Atlantic waters lying just below the surface (< 50 m) even as the surface waters showed some Agulhas influence (Fig. 2a and c). The trailing edge of E1 (station 3) is considered part of the eddy group given its proximity to the eddy centre (where retention of the eddy source waters is typically strongest; Wang et al., 2018) compared to the stations at the leading edge. We note that excluding these three stations (3, 10, and 13) from our analysis does not significantly alter the results. Standard deviations reported for foraminifera- and particulate $\delta^{15}N$ reflect variability between sampled specimens (typically from averaging across multiple stations) rather than analytical error, as the former is generally greater than the latter.

3.3.1 Foraminifer abundance and size

Three dominant foraminifer species were present at all stations sampled in 2017; combined, the deeper-dwelling species, *Globorotalia inflata*, *Globorotalia truncatulinoides*, and *Globorotalia hirsuta* accounted for between 73% and 100% of the total foraminifera at each station (Fig. 6). Atlantic stations 17 (2.6°E) and 14 (5.1°E) were characterised by the highest relative abundances of spinose shallower-dwellers (*Globigerina bulloides*, *Orbulina universa*, and *Globigerina falconensis*) at 26.5% and 18.5% of the total foraminifera. In contrast, stations 13 (7.5°E) and 9 (11.8°E) consisted almost entirely of *G. inflata*, *G. hirsuta*, and *G. truncatulinoides*. We observed none of the typical subtropical species previously recorded in this region (e.g., *Globigerinoides ruber*, *Trilobus sacculifer*, *Globorotalia menardii*; Lončarić, 2006; Kemle-von Mücke and Oberhönsli, 1999; Schiebel and Hemleben, 2017; Bergh and Compton, 2020) apart from a single *G. ruber* specimen at station 14.

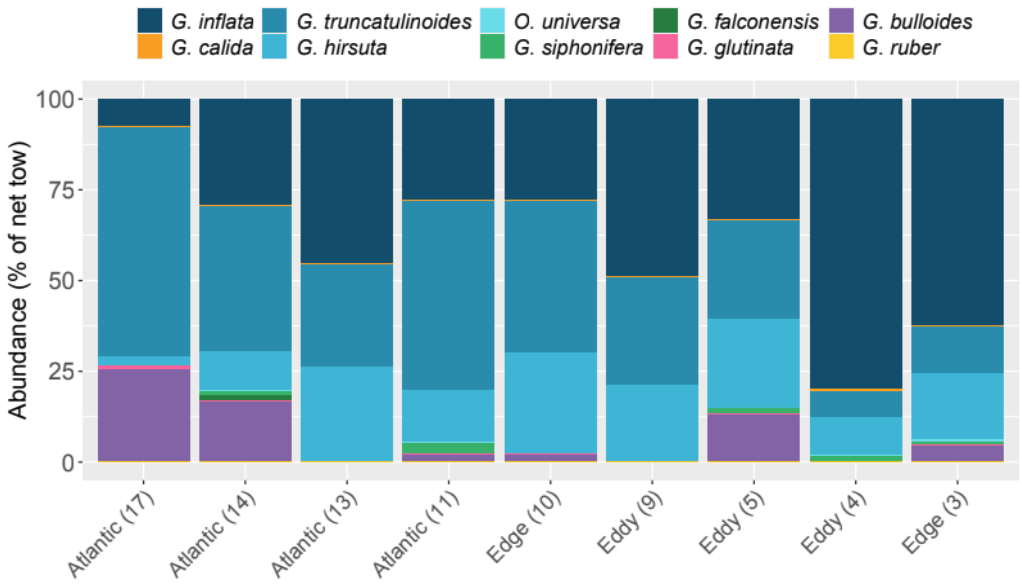

Figure 6. Relative abundance of different species of foraminifera captured in the net tows across the transect. Numbers in parentheses indicate stations. Station 10 at the leading edge of E1 is assigned to the Atlantic group while station 3 at the trailing edge is grouped with the eddy stations (see text for details).

Although the three deeper-dwelling species dominated the foraminiferal assemblage across the transect, their abundances relative to each other varied, with the *G. inflata* and *G. truncatulinoides* proportions varying inversely ($r^2 = 0.89$; $p < 0.01$). *Globorotalia truncatulinoides* dominated the western section of the transect (e.g., 63% of the total assemblage at station 17 where *G. inflata* comprised just 7%), while *G. inflata* dominated in the east (e.g., 80% at station 5 where *G. truncatulinoides* contributed only 7%). The contribution from *G. hirsuta* across the transect was smaller (3 to 28%; lowest in the Atlantic and highest at the leading edge of E1) and did not show a relationship with either the *G. inflata* or *G. truncatulinoides* abundances. Most other species (*O. universa*, *Globigerinella calida*, *Globigerinella siphonifera*, and *G. bulloides*) were present in low numbers at several stations across the transect. *Globigerina falconensis* was only present at two Atlantic stations (13 and 14), as was *Globigerinita glutinata* (stations 14 and 17).

Globorotalia truncatulinoides and *G. hirsuta* were the two largest species sampled across the transect (longest dimensions averaging 614 ± 138 μm and 614 ± 113 μm, respectively), followed by *G. inflata* (507 ± 78 μm). On average, all three of these species were larger at the Atlantic stations than in E1, although the differences were not statistically significant. The opposite trend was observed for the euphotic-dwelling *G. bulloides* and *O. universa*, which were on average slightly larger in E1 than in the Atlantic, although specimen numbers were too low to establish significance.

Figure 7. a) Violin plot showing the concentration-weighted average $\delta^{15}N$ of mixed-layer PON, bulk zooplankton (250-500 μm and 500-1000 μm size classes), and foraminifer tissue

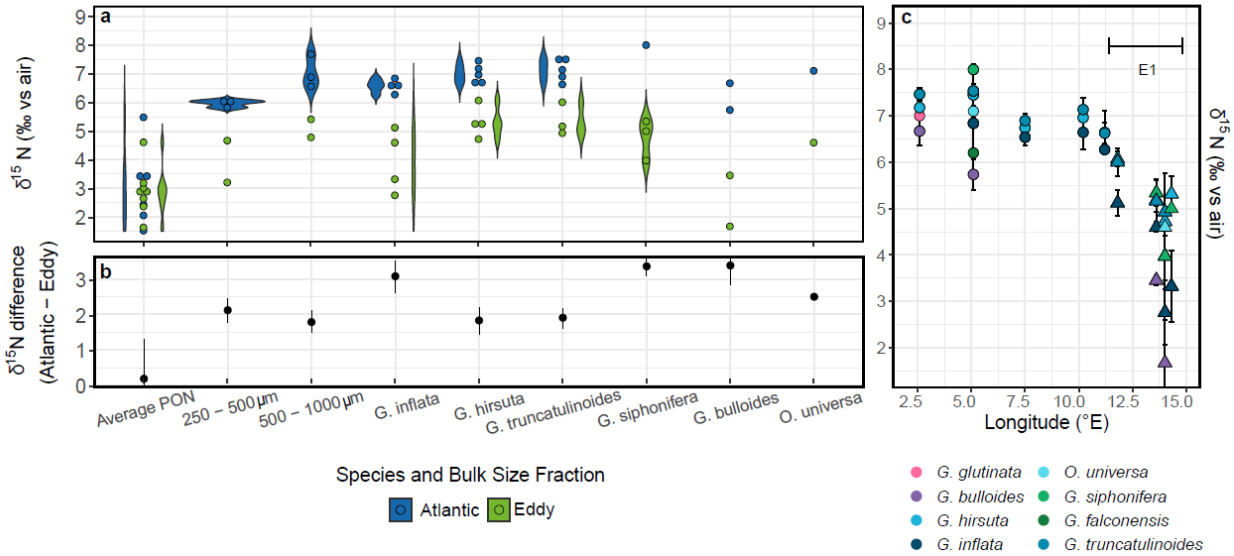

(i.e., FT-δ^{15}N) for six species collected in the 0 - 200 m net tows in 2017. Circles represent the average FT-δ^{15}N measured in triplicate for each species at a single station, with the blue circles indicating Atlantic stations and the green circles showing the data from Agulhas eddy (E1) data. The shapes behind or alongside the circles show the spread of the data; b) The difference in mean FT-δ^{15}N between Atlantic and E1 foraminifera for each particulate pool or foraminifer species; c) Species-specific average FT- δ^{15}N at each station sampled along the transect, with circles and triangles representing Atlantic and eddy stations, respectively.

3.3.2 Foraminifer tissue nitrogen isotopes (FT-δ^{15}N)

For the eddy group, the overall FT-δ^{15}N (i.e., combining data from all species) ranged from 1.7‰ to 6.1‰, with a mean of 4.4 ± 1.2‰ (n = 45) (Fig. 7a). FT-δ^{15}N was significantly higher ($p < 0.01$) at the Atlantic stations (5.7‰ to 8.0‰, mean of 6.8 ± 0.6‰ (n = 63)) and less variable (range of 2.3‰ in the Atlantic, *versus* 4.4‰ in the eddy). The same trends hold for most species (i.e., lower FT-δ^{15}N in the eddy than in the Atlantic samples; Fig. 7b). The mean FT-δ^{15}N of the highly abundant *G. inflata* was 6.7 ± 0.5‰ (n = 14) and 3.6 ± 1.0‰ (n = 12) at the Atlantic and eddy stations, respectively, while the less abundant *G. bulloides* had a mean FT-δ^{15}N of 6.3 ± 0.6‰ (n = 4) in the Atlantic stations and 2.9 ± 0.9‰ (n = 4) in the eddy. Where numerous enough to measure, *G. siphonifera* had a higher FT-δ^{15}N than other species in both the Atlantic and eddy samples (8.0 ± 0.1‰ (n = 3 samples from one station) and 4.6 ± 0.8‰ (n = 7 samples from three stations), respectively). Additionally, *G. hirsuta* and *G. truncatulinoides* were consistently higher in FT-δ^{15}N than co-occurring species at all stations, with an average eddy FT-δ^{15}N of 5.3 ± 0.5‰ (n = 12) and 5.4 ± 0.7‰ (n = 9) and Atlantic FT-δ^{15}N of 7.1 ± 0.4‰ (n = 19) and 7.3 ± 0.5‰ (n = 19), respectively.

3.3.3 Foraminifer shell-bound nitrogen isotopes

Shell-bound $\delta^{15}N$ correlated well with FT-$\delta^{15}N$ for all species ($r^2 = 0.8$; Fig. 8a) and was on average 1.3 ± 0.8‰ higher than FT-$\delta^{15}N$ for the same species at a given station. Shell measurements for the three species present at both the eddy and Atlantic stations (*G. truncatulinoides, G. hirsuta*, and *G. inflata*) yielded an average $\delta^{15}N$ of 6.3 ± 1.4‰ (n = 7) and 7.9 ± 0.7‰ (n = 11), respectively (i.e., an Atlantic-eddy difference of 1.3‰). The spread in the shell-bound $\delta^{15}N$ data was also greater for the eddy (2.4‰) than the Atlantic samples (1.3‰). Similar to FT-$\delta^{15}N$, there was a larger difference between Atlantic and eddy shell samples for *G. inflata* than for *G. hirsuta* or *G. truncatulinoides* (the difference between Atlantic and eddy shell-bound $\delta^{15}N$ was 1.5‰ greater for *G. inflata* than for the other two species; in the case of FT-$\delta^{15}N$, the difference was 1.0‰).

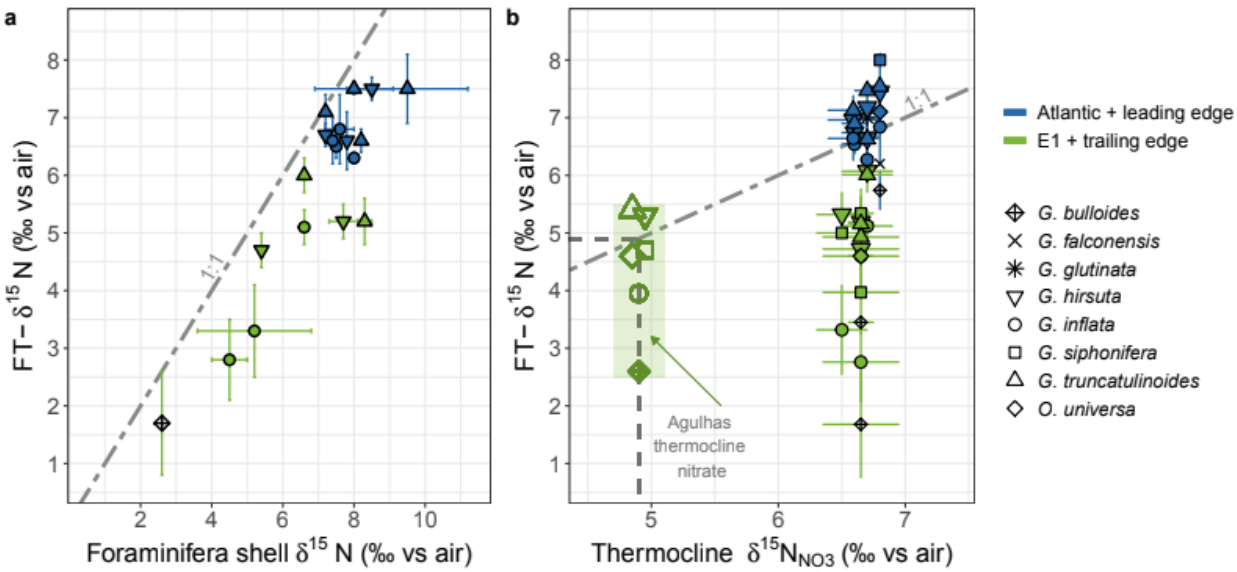

Figure 8. a) Cross-plot of FT-$\delta^{15}N$ versus foraminifer shell-bound $\delta^{15}N$ from the same net tows; b) Comparison of FT-$\delta^{15}N$ and thermocline $\delta^{15}N_{NO3}$ (approximated by the $\delta^{15}N_{NO3}$ measured across the transect. Blue symbols show nitrate and foraminifer measurements from the Atlantic stations and the leading edge of Agulhas eddy E1 while green symbols show data from within E1 and include the trailing edge station (see section 2.4 for details). Error bars show ±1 standard deviation of triplicate measurements of the same foraminifer species at each station (y-axis) and duplicate nitrate isotope measurements from the same station and depth (x-axis). Shapes in the shaded green box indicate where the average eddy FT-$\delta^{15}N$ for each foraminifer species would be positioned if plotted versus the mean Agulhas thermocline $\delta^{15}N_{NO3}$ (4.9‰; calculated for all thermocline data available for the ASCA line (Marshall et al., 2023) rather than from just the representative Agulhas profile shown in Fig. 4b). The dashed grey lines in both figures indicates a slope of 1:1.

3.3.4 Bulk zooplankton and particulate organic N

The $\delta^{15}N$ of the bulk zooplankton (for the combined eddy and Atlantic stations) increased with increasing size-fraction, from a mean of 5.8 ± 0.6‰ for the 250 – 500 µm size-class to 6.7 ± 1.2‰ for the 500 – 1000 µm size-class (Fig. 7a). Both these zooplankton size classes (chosen due to their

containing most of the foraminifera and their larger prey) had a higher $\delta^{15}N$ at the Atlantic (mean of 6.0 ± 0.1‰ (n = 3) and 7.2 ± 0.6‰ (n = 3), respectively) than the eddy stations (3.9 ± 1.0‰ (n = 2) and 5.1 ± 0.4‰ (n = 2), respectively). This equates to an Atlantic-eddy difference of 1.9‰ and 2.0‰ for the 250 – 500 μm and 500 – 1000 μm size classes, respectively, similar to the trends observed for the foraminifera.

We observed no difference in upper-ocean (0-100 m) PON concentrations between the eddy and Atlantic stations (0.3 ± 0.4 μM (n = 7) and 0.3 ± 0.4 μM (n = 6), respectively). Similarly, there was no significant difference in the mean PON-$\delta^{15}N$ between the two groups (2.8 ± 1.6‰ (n = 6) for the Atlantic and 2.5 ± 0.7‰ (n = 7) for the eddy), although the Atlantic samples exhibited larger within-group variability (Fig. 7a, b). Both the lowest and the highest average mixed-layer PON-$\delta^{15}N$ (1.2 ± 0.8‰ and 5.5 ± 0.9‰) were measured at Atlantic stations.

3.3.5 Foraminifer tissue $\delta^{15}N$ *versus* seawater nitrate $\delta^{15}N$

Because we have considerably more measurements (and replicate samples) of FT-$\delta^{15}N$ than shell-bound $\delta^{15}N$, we focus our comparison with $\delta^{15}N_{NO3}$ on the FT-$\delta^{15}N$ data. We nonetheless expect the same trends to apply to the shells given their strong correlation with FT-$\delta^{15}N$ (Fig. 8a; Smart et al., 2018, 2020). Of all the species measured, *G. truncatulinoides*, *G. hirsuta*, and *G. inflata* were most similar in $\delta^{15}N$ to thermocline nitrate at the Atlantic stations (with the mean $\delta^{15}N_{NO3}$ of SASTMW, the water mass just below the mixed layer, taken to represent thermocline nitrate). The combined average FT-$\delta^{15}N$ for *G. truncatulinoides* and *G. hirsuta* was 7.2 ± 0.4‰, compared to a thermocline $\delta^{15}N_{NO3}$ of 6.9 ± 0.4‰ (or 7.0 ± 0.3‰ when comparing only the data from 2017 when the net tows were undertaken) (Fig. 8b).

The similarity of FT-$\delta^{15}N$ to $\delta^{15}N_{NO3}$ did not extend to E1 where *G. truncatulinoides* and *G. hirsuta* had a combined FT-$\delta^{15}N$ that was on average 1.5‰ lower than the local thermocline $\delta^{15}N_{NO3}$ (mean FT-$\delta^{15}N$ of 5.3 ± 0.6‰ *versus* $\delta^{15}N_{NO3}$ of 6.8 ± 0.6‰; Fig. 8b). Across all the eddy stations, *G. bulloides* and *G. inflata* were consistently most different in $\delta^{15}N$ from thermocline nitrate, with their minimum FT-$\delta^{15}N$ (as for all species) observed at station 4 in the centre of E1. The thermocline-to-FT-$\delta^{15}N$ difference for *G. bulloides* and *G. inflata* at this station was 5.0‰ and 3.9‰, respectively. Comparing the mean eddy FT-$\delta^{15}N$ with the $\delta^{15}N_{NO3}$ of the Agulhas thermocline (4.9‰, calculated by averaging all thermocline data available for the ASCA line; Marshall et al., 2023) reveals a strong similarity for *G. truncatulinoides* (5.4 ± 0.7‰), *G. hirsuta* (5.3 ± 0.5‰), *G. siphonifera* (5.3 ± 0.3‰), and *O. universa* (4.6‰), while *G. inflata* and *G. bulloides* were lower in FT-$\delta^{15}N$ than Agulhas thermocline nitrate (3.6 ± 1.0‰ and 2.9 ± 0.9‰, respectively).

4 Discussion

4.1 Absence of Agulhas planktic foraminifer assemblages in the Cape Basin

For samples collected in winter 2017, we observed no robust differences in the foraminifer assemblages inside and outside Agulhas eddy E1. The temperate winter/spring species, *G. truncatulinoides* and *G. hirsuta*, and the more transitional species, *G. inflata*, dominated across the

transect. *G. inflata*, appeared to fare best in more turbulent waters (increasing in relative abundance at the trailing edge of E1). The transect-wide similarity in foraminifer community composition indicates that diagnosing Agulhas leakage through an abundance-based index is not always possible, particularly once Agulhas eddies have migrated some distance from the Retroflection region. Similar foraminifer species homogeneity has been observed for a mature (i.e., >9 month-old) Agulhas ring and its Cape Basin surrounds during late summer (Schouten et al., 2000; Froyland et al., 2015), with the (sub)tropical/warm-water species, *T. sacculifer* and *G. ruber* (both considered Agulhas leakage fauna), dominating inside and outside the eddy (Lončarić, 2006).

Seasonality is likely the primary determinant of the "background" foraminifer assemblage of the Cape Basin (Van Aken et al., 2003; Peeters et al., 2004), as is the case for other ocean regions (Boltovskoy, 1994; Eguchi et al., 2003; Jonkers and Kučera, 2017). Recently-shed eddies can disrupt this scenario, however, as the upper-ocean temperatures of young Agulhas rings and eddies are warmer than the Cape Basin, creating a temporary niche for (sub)tropical foraminifer species in the southeast Atlantic. Eddies located near the Retroflection tend to be relatively young (<5 months), characterized by large SST and SSH anomalies, but in a stage of active decay (Schouten et al., 2000). Thus, intense heat loss and advective mixing rapidly cool eddy surface waters, particularly as they near the South Atlantic subtropical gyre (Duncombe Rae, 1991; Goni et al., 1997; De Ruijter et al., 1999; Van Aken et al., 2003). The mean annual SST at 28°E in the Agulhas Current is ~23°C (Garcia et al., 2019); further west and closer to the Retroflection at 18.5°E, SST decreases to ~19°C (Locarini et al., 2013). By the time E1 reached our SAMBA transect (7 to 8 months after shedding), its SST had dropped to 16°C. Although within the temperature range determined under laboratory conditions to be acceptable to (sub)tropical foraminifer species (e.g., *T. sacculifer*, *G. ruber*, *N. dutertrei*; Bijma et al., 1990), the E1 SST was nonetheless below that considered optimal for these species to reproduce (i.e., above 20°C for all three species; Hecht, 1976; Waterson et al., 2017). In the summer, however, SSTs in the Cape Basin rise above 20°C (Lea et al., 2018), which is adequate to at least temporarily sustain (sub)tropical foraminifer populations imported by Agulhas rings (Peeters et al., 2004; Lončarić, 2006).

Among the (more temperate) foraminifer species present in E1, the variations in relative abundance might reflect their preferences for different hydrographic conditions (Feldmeijer et al., 2015). The high percentage of *G. inflata* within and at the trailing edge of E1 relative to the Atlantic stations (Fig. 6) is consistent with previous assertions that this species is more tolerant of vertical mixing and rapidly changing conditions (Deuser et al., 1981; Chapman, 2010; Schiebel and Hemleben, 2017; Kretschmer et al., 2018). In contrast, *G. truncatulinoides* was most abundant at stations located near the comparatively stable South Atlantic subtropical gyre.

4.2 Origin of the distinct Agulhas eddy isotope ratios

As the dominant form of fixed N in the ocean, nitrate sets the baseline for the N isotope distributions in an ecosystem. The lower $\delta^{15}N_{NO3}$ (and Δ(15-18)) in the mixed layer at the eddy stations relative to the background South Atlantic (Fig. 4b, 5) suggests that the controls on the nitrate isotope distributions in eddy waters are distinct, and that eddies may receive a low-$\delta^{15}N_{NO3}$ source that is not available to the surrounding Atlantic mixed-layer. We examine the possibilities in detail below.

4.2.1 Limited role of phytoplankton nitrate assimilation

One mechanism that can cause mixed-layer $\delta^{15}N_{NO3}$ to vary is the extent to which vertically-supplied nitrate is assimilated by phytoplankton. Phytoplankton preferentially consume ^{14}N-bearing nitrate, such that the $\delta^{15}N_{NO3}$ of partially-assimilated nitrate rises as its concentration declines (Minagawa and Wada, 1986; Sigman et al., 1999). Thus, the more completely a particular supply of nitrate has been consumed, the higher its $\delta^{15}N_{NO3}$, and vice versa. It is therefore possible that the lower $\delta^{15}N_{NO3}$ in the eddy mixed layer relative to the background Atlantic was due to less complete consumption of the same nitrate supply.

At first glance, the cruise nitrate concentration data appear consistent with this idea. An east-west gradient is apparent in both the 2015 and 2017 measurements, with surface nitrate concentrations declining near-linearly from the nearshore (~3 μM) to the most offshore station (0.8 μM at 0°E) (Fig. S1). In 2017, E1 was located at the eastern edge of the transect and its mixed layer hosted higher nitrate concentrations (by ~0.4 μM) than the Atlantic stations to the west. One might thus conclude that the mixed-layer $\delta^{15}N_{NO3}$ (and by extension, the FT-$\delta^{15}N$) difference between the eddy and Atlantic stations can be explained by a lower degree of nitrate consumption to the east (eddy) *versus* the west (Atlantic) of the transect.

However, our sampling occurred near the beginning of the nitrate resupply period (Fig. 3), such that the mixed layer nitrate concentration and $\delta^{15}N_{NO3}$ will mainly reflect ongoing mixing of thermocline nitrate with a small volume of nitrate-depleted surface water left over from the previous growing season (i.e., late-summer/autumn). By contrast, because the lifetime of zooplankton and foraminifera is weeks to months (Montoya et al., 2002; Schiebel and Hemleben, 2005; Loick-Wilde et al., 2016), their biomass $\delta^{15}N$ will largely reflect the N consumed over the previous growing season, prior to the onset of nitrate resupply. In other words, there is likely a temporal decoupling between the nitrate present in the surface layer (although not the subsurface) at the time of our sampling and the zooplankton and foraminifera biomass. The longer residence time of zooplankton and foraminifera relative to phytoplankton (represented here by the bulk PON; residence time of days to weeks) likely also explains the lack of $\delta^{15}N_{PON}$ difference between the eddy and Atlantic stations (see section 4.3.4).

Notwithstanding a temporal decoupling between surface nitrate and foraminifera, the CMEMS concentration data suggest that the fraction of the nitrate supply remaining in the surface (i.e., $[NO_3^-]_{(July,\ mixed\ layer)}/[NO_3^-]_{(Sept/Oct,\ supply)}$) was relatively constant across the transect (64-67%), rather than lower to the east than the west as would be required to explain the $\delta^{15}N_{NO3}$ data by differential nitrate consumption. Furthermore, during the 2015 cruise, Agulhas eddies were encountered further west, and their mixed-layer nitrate was on average 0.7 μM lower than in the Atlantic mixed layer. This should have resulted in a higher $\delta^{15}N_{NO3}$ in the eddy mixed layers than the background Atlantic if the trend in $\delta^{15}N_{NO3}$ was driven by nitrate consumption. Instead, eddy mixed-layer $\delta^{15}N_{NO3}$ in 2015 was 2.3‰ lower than the average Atlantic mixed-layer $\delta^{15}N_{NO3}$, consistent with the eddy-Atlantic difference observed in 2017.

Finally, if the difference in the $\delta^{15}N_{NO3}$ between the eddy and background Atlantic was due to differential nitrate consumption, the $\delta^{18}O_{NO3}$ should be similarly variable since $\delta^{15}N_{NO3}$ and $\delta^{18}O_{NO3}$ increase proportionally during nitrate assimilation (Granger et al., 2004, 2010; Rohde et al., 2015). However, we observe a much smaller (statistically insignificant; $p = 0.2$) difference in the mean $\delta^{18}O_{NO3}$ in the mixed layer of the eddy *versus* the background Atlantic (6.1 ± 1.3‰ *versus* 6.6 ± 2.1‰, Fig. S2), which strongly suggests that nitrate assimilation is not the dominant driver of the eddy-Atlantic difference in $\delta^{15}N_{NO3}$.

Below the depth of winter mixing (~300 m), nitrate Δ(15-18) averages 3.2 ± 0.2‰ for all stations across the transect, consistent with previous observations for SAMW in the South Atlantic (Tuerena et al., 2015; Marconi et al., 2019; Flynn et al., 2020). At the background Atlantic stations, mixed-layer nitrate Δ(15-18) was 3.0 ± 1.4‰, indistinguishable from the subsurface nitrate and indicating that the main driver of the nitrate isotope distributions in the Atlantic mixed layer is the seasonal supply and consumption of the subsurface nitrate pool (Granger et al., 2004; Rafter et al., 2013). By contrast, mixed-layer nitrate Δ(15-18) in the eddies was low (average of 1.8 ± 1.2‰) and similar to the mean Δ(15-18) observed in the Agulhas Current thermocline and mixed layer (2.1‰ and 1.3‰, respectively; Fig. 5; Marshall et al., 2023). We thus conclude that a mechanism other than differential nitrate consumption is required to explain the lower nitrate $\delta^{15}N_{NO3}$ and Δ(15-18) in Agulhas eddies *versus* the background Atlantic.

4.2.2 Transported signals: N_2 fixation and co-occurring nitrate assimilation and nitrification

N_2 fixation introduces organic N to the mixed layer that is low in $\delta^{15}N$, -2‰ to 0‰ (Hoering and Ford, 1960; Minagawa and Wada, 1986). The subsequent sinking and remineralization of this organic N yields subsurface nitrate that is similarly low in $\delta^{15}N$ (Knapp et al., 2005, 2008; Marshall et al., 2023). By contrast, the $\delta^{18}O$ of newly nitrified nitrate is relatively high, as it is set by the $\delta^{18}O$ of seawater (~0‰) plus an isotopic offset of ~1.1‰ (Sigman et al., 2009; Boshers et al., 2019; Buchwald and Casciotti, 2013). As such, N_2 fixation causes both the $\delta^{15}N_{NO3}$ and the Δ(15-18) of nitrate to decline (Sigman et al., 2009; Rafter et al., 2013). Data from the Agulhas Current (Fig. 4; Marshall et al., 2023) and the waters of the southern Indian Ocean (Harms et al., 2019) that feed the Agulhas Current have a low $\delta^{15}N_{NO3}$ and Δ(15-18) throughout the thermocline (4.9‰ and 2.4‰, respectively) and low Δ(15-18) in surface waters (1.3‰). The similarity of the eddy and Agulhas Current Δ(15-18) strongly suggests that Agulhas leakage transports recently fixed nitrate from the South Indian Ocean into the Cape Basin. The potential vorticity and kinematic steering associated with the circulation of migrating eddies (Chelton et al., 2011; Condie and Condie, 2016) likely help to maintain the isotopic distinction between the eddy and the surrounding South Atlantic.

Thermocline $\delta^{15}N_{NO3}$ is robustly low across the Agulhas Current region (Harms et al. 2019; Marshall et al., 2023) yet within Agulhas eddies, subsurface $\delta^{15}N_{NO3}$ is generally more similar to the $\delta^{15}N_{NO3}$ of the South Atlantic thermocline (i.e., SASTMW). The absence of low-$\delta^{15}N_{NO3}$ in the eddy thermocline can be attributed to deep convective mixing of Agulhas mixed-layer and thermocline waters at the Retroflection and within Agulhas eddies (Dufois et al., 2016; Olson et al., 1992; Schmitt and Olson, 1985; Marshall et al., 2023). In addition, the consumption of this low-$\delta^{15}N$ Agulhas nitrate by phytoplankton in the eddy mixed layer will rapidly raise its $\delta^{15}N_{NO3}$ (and $\delta^{18}O_{NO3}$), overprinting the low $\delta^{15}N_{NO3}$ but not the low Δ(15-18) characteristic of the Agulhas Current/southwest Indian Ocean thermocline (Marshall et al., 2023).

The low nitrate Δ(15-18) in the eddies may also be influenced by coupled partial nitrate assimilation and nitrification. If nitrate assimilation and nitrification co-occur (e.g., at the base of the mixed layer; Fawcett et al., 2015; Marshall et al., 2023), the cycling between organic N and nitrate yields no net change in the $\delta^{15}N_{NO3}$ of the combined (i.e., partially assimilated plus newly-nitrified) nitrate pool, provided that N is neither lost nor gained (Rafter et al., 2013; Sigman et al., 2005, 2009). By contrast, assimilation is a sink for the O atoms in nitrate while nitrification is a source, with the $\delta^{18}O_{NO3}$ reset by nitrification to ~1.1‰ (Sigman et al., 2009; Buchwald and

Casciotti, 2013; Boshers et al., 2019). As such, coupled partial nitrate assimilation and nitrification causes the $\delta^{18}O_{NO3}$ of the combined nitrate pool to rise, which, along with the lack of change in $\delta^{15}N_{NO3,}$ drives a decline in Δ(15-18) (Sigman et al., 2005, 2009; Wankel et al., 2007; Rafter et al., 2013; Fawcett et al., 2015; Deman et al., 2021; Marshall et al., 2023). Nitrification of partially assimilated N at the base of the mixed layer could occur prior to and/or following eddy spawning, making the low-Δ(15-18) either a transported or *in situ* signal, or both. Indeed, it has been suggested that some portion of the low-Δ(15-18) nitrate in the mixed layer and upper thermocline of the Agulhas Current (Fig. 5) derives from *in situ* coupled partial nitrate assimilation and nitrification (Marshall et al., 2023). Our data indicate that this signal is then transported (and possibly augmented) in Agulhas leakage. Coupled partial nitrate assimilation and nitrification cannot account for the entire lowering of the nitrate Δ(15-18), however, either in the Agulhas Current or in the eddy, as this mechanism does not lower $\delta^{15}N_{NO3}$. Thus, there must be a role for N_2 fixation in driving the nitrate isotope distributions observed in Agulhas leakage.

4.2.3 In-eddy N-cycling processes: N_2 fixation and ammonium recycling

Above, we argue that the low foraminifer (and bulk zooplankton) $\delta^{15}N$ in the eddy reflects the lower $\delta^{15}N_{NO3}$ of Agulhas-sourced waters relative to the background Atlantic. In-eddy FT-$\delta^{15}N$ may also be affected by *in situ* processes that further decrease the $\delta^{15}N_{NO3}$ (and Δ(15-18)) of eddy nitrate, resulting in a corresponding decline in the $\delta^{15}N$ of foraminifera (and other plankton) in Agulhas eddies during their migration into the South Atlantic (i.e., after spawning). Anticyclonic eddies in other subtropical and mid-latitude regions have been observed to host elevated rates of N_2 fixation (Holl et al., 2007; Fong et al., 2008; Löscher et al., 2016; Liu et al., 2020); similar conditions in the Cape Basin may favour N_2 fixation, provided that the iron supply is sufficient (Deutsch et al., 2007; Marshall et al., 2022; Martin et al., 2024). Agulhas eddies do appear to host higher trace metal concentrations than the surrounding Atlantic because they include a significant contribution of southwest Indian Ocean coastal waters (Paul et al., 2015; Conway et al., 2016; Samanta et al. 2023). However, the $\delta^{15}N_{NO3}$ and Δ(15-18) of nitrate in the eddy mixed-layer and thermocline is higher than in the Agulhas Current (Fig. 4b, 5), which suggests that if N_2 fixation does occur in Agulhas eddies, its influence on $\delta^{15}N_{NO3}$ is relatively minor.

Another mechanism that could lower foraminifer $\delta^{15}N$ is the recycling of low-$\delta^{15}N$ ammonium within the eddy. Ammonium produced via zooplankton excretion and bacterial decomposition of organic matter has a lower $\delta^{15}N$ (by ~5‰) than nitrate (Checkley and Miller, 1989; Mobius, 2013); when assimilated by phytoplankton, this ammonium decreases the $\delta^{15}N$ of PON (Altabet 1988; Fawcett et al., 2011; Treibergs et al., 2014) and subsequently, the $\delta^{15}N$ of foraminifera that feed on PON (Smart et al., 2020). Enhanced reliance of phytoplankton on regenerated N in anticyclonic eddies has previously been suggested in response to light limitation induced by their characteristically deep mixed layers (Dortch, 1990; Siegel et al., 1995). Indeed, Wallschuss et al. (2022) measured nitrification rates in the mixed layer of E1 that were an order of magnitude higher than in the surrounding Atlantic. This finding indicates that (1) the deep mixed-layer of E1 was conducive to intense N recycling, and (2) the eddy phytoplankton were light-limited, a condition that favours reliance on regenerated N, which is energetically cheaper to assimilate than nitrate (Dortch, 1990). It is thus likely that ammonium recycling during eddy transit contributed to the low $\delta^{15}N$ of the foraminifera in E1.

Regardless of whether N_2 fixation or ammonium recycling were active during eddy transit, our nitrate isotope data indicate that the $\delta^{15}N_{NO3}$ and Δ(15-18) of mixed-layer nitrate in Agulhas

leakage are strongly influenced by processes occurring in the Agulhas Current and its source waters, and as such, are distinct from the surrounding Cape Basin. While the low $\delta^{15}N_{NO3}$ signal is rapidly eroded by nitrate assimilation during eddy migration, its influence persists in the $\delta^{15}N$ of other eddy N pools. Moreover, the low nitrate Δ(15-18) is retained, making this parameter a robust tracer of Agulhas leakage (Marshall et al. 2023).

4.3 Controls on foraminifer $\delta^{15}N$

All foraminifer species in E1 were significantly lower in FT-$\delta^{15}N$ than the Atlantic foraminifera (4.4 ± 1.2‰ *versus* 6.8 ± 0.6‰; Figs. 7 and 8). We observe the same trend for the foraminifer shells (6.3 ± 1.4‰ *versus* 7.9 ± 0.7‰), as well as for tissue and shell-bound N within the same species, suggesting that the eddy community was supported by a lower-$\delta^{15}N$ diet. The similar Atlantic-eddy $\delta^{15}N$ difference observed for bulk zooplankton in the foraminifer size range (7.2 ± 0.6‰ *versus* 5.1 ± 0.4‰) supports this notion. Nitrate supplied to the winter mixed layer of the South Atlantic was completely consumed by phytoplankton during the spring/summer growth season preceding our sampling (Fig. 3). This nitrate consumption would have generated mixed-layer PON that was similar in $\delta^{15}N$ to the subsurface nitrate supply (Mariotti et al., 1981). As such, in-eddy PON produced from the consumption of Agulhas nitrate would have been lower in $\delta^{15}N$ (~4.9‰) than PON outside the eddy that was fuelled by SASTMW nitrate (~6.9‰). Since all planktic foraminifera and zooplankton consume some form of particulate N (Bé and Hutson, 1977; Spindler et al., 1984; Uhle et al., 1997; Bird et al., 2020), those inhabiting the eddy must have incorporated the low $\delta^{15}N$ of Agulhas nitrate into their biomass. The lower $\delta^{15}N$ of foraminifera (tissue and shell) in the eddy *versus* the background Atlantic is thus consistent with the eddy fauna recording the $\delta^{15}N$ of Agulhas thermocline nitrate while foraminifera in background Atlantic waters reflect the higher $\delta^{15}N$ of SASTMW.

In contrast to the zooplankton and foraminifera, the $\delta^{15}N$ of contemporaneously-collected mixed-layer PON was not robustly different between the eddy and the background Atlantic. We attribute this lack of isotopic difference to the comparatively short integration time of much of the suspended PON pool (that we assume comprised mainly phytoplankton) compared to zooplankton in general and foraminifera in particular (Eppley et al., 1983; Altabet and McCarthy, 1985; Fasham et al., 1990; Capone et al., 2008). Indeed, $\delta^{15}N_{PON}$ can be rapidly altered (within hours to days; Savoye et al., 2003; Treibergs et al. 2014) by several processes, including a switch in the dominant N form consumed by phytoplankton (i.e., from nitrate to ammonium) (Liu et al., 2007; Treibergs et al. 2014) and mixing with surrounding water masses (Mino et al., 2020; Haas et al., 2022). The isotopes of suspended PON are further discussed in section 4.3.4 below.

4.3.1 Interspecies relationships

We found broadly consistent interspecies FT-$\delta^{15}N$ relationships across the eddy and Atlantic stations that are largely in agreement with previous observations (Ren et al., 2009, 2012; Li et al., 2019; Smart et al., 2018, 2020). Higher FT-$\delta^{15}N$ is associated with deep-dwelling non-spinose species (*G. truncatulinoides* and *G. hirsuta*, typically inhabiting depths > 100 m; Reynolds et al., 2018), the FT-$\delta^{15}N$ of *G. inflata* (a mid- to shallow-depth dwelling non-spinose species) is slightly lower (by 1‰ on average), and the FT-$\delta^{15}N$ of *G. bulloides* and *G. falconensis* (spinose shallow dwellers) is the lowest (on average 1.9‰ lower than the FT-$\delta^{15}N$ of *G. truncatulinoides*) (Table

1). This pattern closely resembles that reported for the Southern Ocean (where FT-δ^{15}N of *G. truncatulinoides*/*G. hirsuta* > *G. inflata* > *G. bulloides*; Smart et al., 2020). Differences in FT-δ^{15}N among species are likely a reflection of both diet and species-specific metabolic processes. For example, *G. truncatulinoides* and *G. hirsuta* are thought to predominantly graze on sinking and subsurface suspended PON (Bé and Hutson, 1977; Sen Gupta, 2003), which is high in δ^{15}N due to the preferential decomposition of ^{14}N-bearing material by heterotrophic bacteria (Altabet, 1988; Mobius, 2013).

Species	**Atlantic FT-δ^{15}N (‰)**	**Eddy FT-δ^{15}N (‰)**	**Estimate of average living depth* (m)**	**Symbionts**
G. bulloides	6.3 ± 0.6	2.9 ± 0.9	0 – 100	No
G. falconensis	6.2 ± 0.0	-	50 – 100	Facultative (unknown)
G. glutinata	7.0 ± NA	-	0 – 80	Facultative (chrysophytes)
G. hirsuta	7.1 ± 0.4	5.3 ± 0.5	100 – 200	No
G. inflata	6.7 ± 0.5	3.6 ± 1.0	80 – 100	Facultative (chrysophytes)
G. siphonifera	8.0 ± 0.1	5.3 ± 0.3	80 – 100	Facultative (chrysophytes)
G. truncatulinoides	7.3 ± 0.5	5.4 ± 0.7	80 – 200**	No
O. universa	7.1 ± NA	4.6 ± NA	70 – 100	Obligate (dinoflagellates)

Table 1. Mean FT-δ^{15}N of the various foraminifer species measured in this study, in the background Atlantic and inside the Agulhas eddy, along with their average living depth. *The average living depth was estimated from Peeters and Brummer, (2002), Sousa et al., (2014), Rebotim et al., (2017), Schiebel and Hemleben (2017), Meilland et al., (2018, 2019), and Lessa et al., (2020). ****G. truncatulinoides* experiences large seasonal vertical displacement and can at times be found at depths > 600 m (Lohmann and Schweitzer, 1989; Cléroux et al., 2007; Feldmeijer et al., 2014; Reynolds et al., 2018 and references therein).

Interestingly, *G. siphonifera* had a similar FT-δ^{15}N to the deep-dwellers despite its hosting symbionts (Gastrich, 1987; Faber et al., 1988), which might be expected to lower its FT-δ^{15}N (Ren et al., 2012). This observation is consistent with tissue and shell measurements from the Sargasso Sea, where the δ^{15}N of *G. siphonifera* was as high or higher than that of the deep-dwelling foraminifera (Smart et al., 2018). In that study it was posited that the chrysophyte symbionts of *G. siphonifera* might be less active in N cycling with the host foraminifera than the dinoflagellates possessed by other symbiotic species (e.g., *G. ruber*), rendering *G. siphonifera* more reliant upon predation and leading to its higher than expected δ^{15}N. Consumption of higher-δ^{15}N food sources available at the dwelling depth of *G. siphonifera* (i.e., at times, sub-euphotic zone; Rebotim et al. 2017; Meilland et al., 2019) may have also contributed to its elevated FT-δ^{15}N (Li et al., 2019).

The dinoflagellate-bearing *O. universa* has previously been observed to be lower in δ^{15}N than non-symbiont-hosting species, despite its diet consisting of higher trophic-level prey (i.e., through predation on other zooplankton; Bé et al., 1977; Spindler et al., 1984). This low δ^{15}N has been explained by symbiont-facilitated retention and recycling of low-δ^{15}N ammonium normally

excreted by foraminifera (Uhle et al., 1999; Ren et al., 2012; Lekieffre et al., 2020). However, we measure an FT-δ^{15}N for *O. universa* (present at stations 4 and 14) that is similarly high to that of the symbiont-barren, deep-dwelling species, *G. hirsuta* and *G. truncatulinoides* (Table 1). This elevated FT-δ^{15}N may indicate a more carnivorous diet for *O. universa* in our system. Alternatively, conditions may have been unfavourable for symbiont photosynthesis (and thus ammonium retention) in the wintertime Cape Basin (e.g., deep mixed layers and elevated turbulence), as has previously been suggested for Sargasso Sea foraminifera in winter (Smart et al., 2018), resulting in the FT-δ^{15}N of *O. universa* converging on that of non-dinoflagellate bearing foraminifera.

The different amounts by which the FT-δ^{15}N (and shell-bound δ^{15}N) of the various foraminifer species are lower in the eddy than the Atlantic (i.e., the "FT-δ^{15}N offset") provides an upper bound on the δ^{15}N excursion we might expect to see in the sediments (e.g., inside *versus* outside the main corridor of Agulhas leakage). The similar FT-δ^{15}N offset for the two non-spinose deep dwellers (1.9‰ and 1.8‰ for *G. truncatulinoides* and *G. hirsuta*, respectively) is likely explained by their similar depth habitat and a common food source. Likewise, the similar (and larger) FT-δ^{15}N offset for *G. inflata* and *G. bulloides* (2.9‰ and 3.4‰, respectively) suggests a similar depth habitat (and thus access to similar food sources), as has been observed for these two species in nutrient-rich regions (Mohtadi et al., 2007; Salgueiro et al., 2020; Zarkogiannis et al., 2020). The larger FT-δ^{15}N offset for these and other shallow- to intermediate-depth dwellers (including *G. siphonifera*) compared to *G. truncatulinoides* and *G. hirsuta* could be linked to their faster isotope turnover times (i.e., shorter lifespans and/or faster metabolisms) and/or their inhabiting a restricted depth range within the eddy (e.g., upper 100 m, Table 1), leading them to incorporate the low-δ^{15}N signature of the eddy more quickly. For example, *G. bulloides*, commonly found in the upper 100 m (Peeters and Brummer, 2002; Jonkers et al., 2013), appears to reproduce monthly (Schiebel et al., 1997), in contrast to the annual reproductive cycle of *G. truncatulinoides* (Hemleben et al., 1985; Lohmann and Schweitzer, 1990). Moreover, some of the deeper-dwelling foraminifera sampled within the eddy may have been recently entrained from greater depths (where they likely consumed a higher δ^{15}N food source), effectively "diluting" the FT-δ^{15}N offset of these species. Nonetheless, a substantial FT-δ^{15}N offset (> 2‰) persisted in all the species studied here, which is encouraging for the development of an Agulhas leakage proxy based on foraminifer-bound δ^{15}N. If seasonally resolved sampling continues to show large FT-δ^{15}N offsets for *G. bulloides* (3.4‰ in this study), it would argue for this species as a prime target for future leakage reconstructions.

4.3.2 Relationship between FT-δ^{15}N and $\delta^{15}N_{NO3}$

At the Atlantic stations, the average FT-δ^{15}N of the three most abundant foraminifer species (*G. truncatulinoides*, *G. hirsuta*, *G. inflata*; all deep and/or mid-depth dwellers) closely resembled the thermocline $\delta^{15}N_{NO3}$ (i.e., offset by only 0.4 ± 0.3‰; Fig. 8b). A similar pattern was observed in the Sargasso Sea, but in that case it was the euphotic-dwelling, symbiont-hosting species, *G. ruber*, *T. sacculifer*, and *O. universa*, that most closely matched $\delta^{15}N_{NO3}$ while the FT-δ^{15}N of the deep dwelling foraminifera was ~1‰ higher (Smart et al., 2018). A comparison of thermocline $\delta^{15}N_{NO3}$ and foraminifera-bound δ^{15}N from surface sediments across the low-mid latitude ocean similarly revealed a lower δ^{15}N for symbiont-hosting foraminifera than for non-symbiotic, deeper-dwelling species (Ren et al., 2012). In that study, the authors reasoned that the dinoflagellate symbionts in shallow-dwelling foraminifera were responsible for the similarity between foraminifer δ^{15}N and thermocline $\delta^{15}N_{NO3}$ as they retain (low-δ^{15}N) ammonium, thereby offsetting the isotopic

enrichment expected for a consumer relative to its diet (DeNiro and Epstein, 1981; Minagawa and Wada, 1984; Montoya et al., 1990). In our study, the FT-δ^{15}N of the facultatively symbiotic *G. inflata* and potentially symbiotic *G. falconensis* (Gastrich, 1987; Jonkers and Kučera, 2015) was slightly lower (0.5‰ to 0.8‰) than thermocline $\delta^{15}N_{NO3}$, seemingly at odds with these earlier findings. However, in the short-term, FT-δ^{15}N is set by the δ^{15}N of the foraminifer diet and species-specific metabolism (e.g., Bird et al., 2020) rather than by $\delta^{15}N_{NO3}$ directly. In the Southern Ocean, for example, seasonal changes in PON δ^{15}N appear to drive large deviations (up to 4‰) in FT-δ^{15}N relative to both the annual average FT-δ^{15}N and the δ^{15}N of the nitrate supply (Smart et al., 2020). As such, the fact that we only have winter data for the South Atlantic may explain the apparently anomalous relationship of the FT-δ^{15}N of certain foraminifer species to $\delta^{15}N_{NO3}$.

The similarity between FT-δ^{15}N and thermocline $\delta^{15}N_{NO3}$ observed at the Atlantic stations did not hold in the eddy. Here, FT-δ^{15}N was on average 2‰ lower than the $\delta^{15}N_{NO3}$ of SASTMW nitrate and was more similar to the $\delta^{15}N_{NO3}$ of the Agulhas thermocline (Fig. 9). As outlined in section 4.2, we suggest that as the eddy migrated into the South Atlantic, nitrate originating in the Agulhas Current thermocline (and mixed layer, although its concentration in this layer would have been extremely low; Marshall et al., 2023) was incorporated into the eddy's deepening mixed layer where it would have been rapidly consumed by phytoplankton and thus integrated into the eddy's planktonic ecosystem. In other words, the waters underlying the eddy mixed layer at the time of our sampling did not reflect the original nitrate supply to its surface ecosystem although the δ^{15}N of the foraminifera and zooplankton did. Given the age of the eddy, along with its retentive anticyclonic circulation and the considerably longer lifetime of foraminifera compared to phytoplankton (i.e., PON), SASTMW nitrate likely contributed only minimally to the FT-δ^{15}N measured in the eddy.

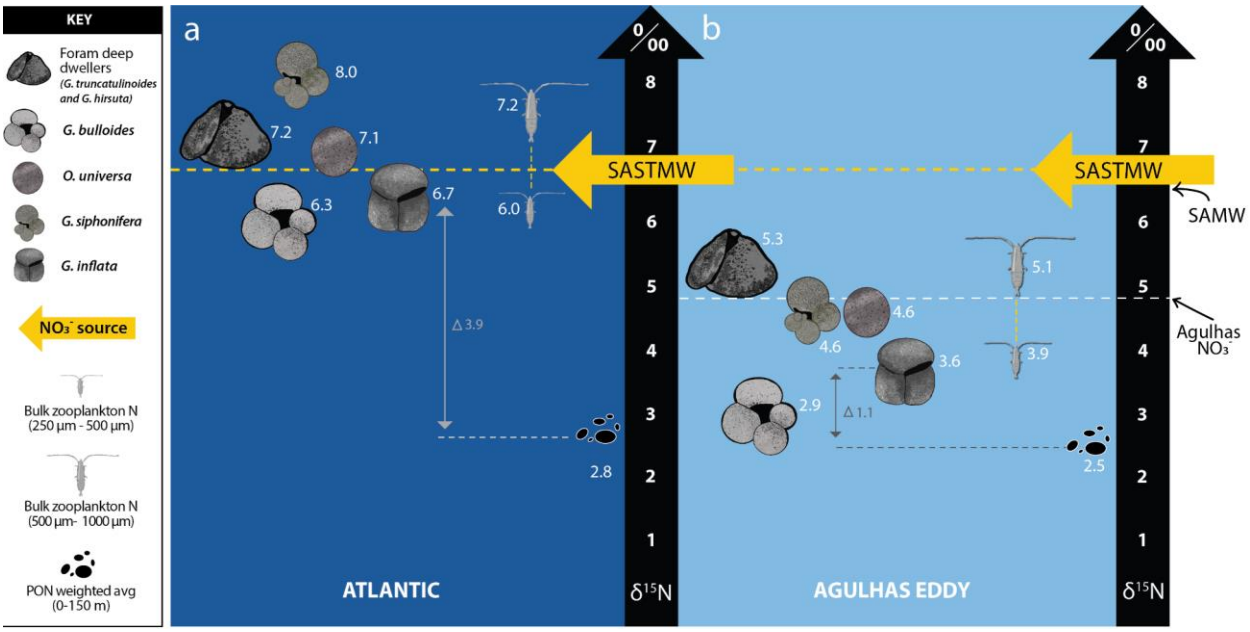

Figure 9. Schematic showing the nitrogen isotope dynamics that we propose were ongoing in a) the background Atlantic and b) an Agulhas eddy sampled in the Cape Basin in 2017, with δ^{15}N shown by the vertical black arrows. The horizontal yellow arrows and dashed lines indicate South Atlantic Subtropical Mode Water (SASTMW, $\delta^{15}N_{NO3}$ of 6.9‰), which is the

water mass (and nitrate supply) located directly below the mixed layer across the Cape Basin. The arrows in panel b show the mean $\delta^{15}N_{NO3}$ of Agulhas Current thermocline nitrate ($\delta^{15}N_{NO3}$ of 4.9‰) and Subantarctic Mode Water (SAMW, $\delta^{15}N_{NO3}$ of 6.7‰, Marshall et al., 2023), which underlies the thermocline and is the ultimate source of nitrate to both the Cape Basin and Agulhas region. Suspended PON $\delta^{15}N$, bulk zooplankton $\delta^{15}N$ (for the 250 – 500 µm and 500 – 1000 µm size classes), and FT-$\delta^{15}N$ are shown using symbols and images of the various species (see legend). The numbers next to the organisms indicate their biomass $\delta^{15}N$, in units of ‰. The thin vertical arrows show the calculated difference (Δ) $\delta^{15}N$ between an example foraminifer species (*G. inflata*; chosen due to its high abundance across the transect and its mid-range trophic position) and the suspended PON.

4.3.3 Relationship between foraminifer $\delta^{15}N$ and PON $\delta^{15}N$

Above, we have compared FT-$\delta^{15}N$ to $\delta^{15}N_{NO3}$. However, foraminifera do not consume nitrate, but rather the photosynthetic biomass generated from the assimilation of nitrate and other N forms, as well as heterotrophic and detrital organic matter (collectively, the suspended PON pool). A recent study from the Southern Ocean showed that FT-$\delta^{15}N$ is more closely tied to the $\delta^{15}N$ of PON than to $\delta^{15}N_{NO3}$ on seasonal timescales (Smart et al., 2020). As such, for the eddy foraminifera to acquire their lower FT-$\delta^{15}N$, they would have had to consume a different (i.e., lower-$\delta^{15}N$) PON pool from the Atlantic foraminifera, which we propose ultimately derived from the assimilation of Agulhas-sourced nitrate. Yet, at the time of sampling, the $\delta^{15}N$ of upper mixed-layer PON in E1 was similar to the PON collected at the Atlantic stations (2.5 ± 0.7‰, n = 7 stations *versus* 2.8 ± 1.6‰, n = 6, respectively).

To explain the suspended PON data, we consider the timescales over which the isotopic signal of the different N pools integrate and examine the potential effect(s) of circulation and seasonality. Phytoplankton, a large component of the PON pool, live for hours to days, which allows for rapid changes to their biomass $\delta^{15}N$ (Pasquero, 2005; d'Ovidio et al., 2010; Treibergs et al., 2014). Suspended PON in the eddy may therefore reflect recent phytoplankton N assimilation (likely of a combination of recycled ammonium and vertically- and/or laterally-supplied Cape Basin nitrate), while foraminifer shell $\delta^{15}N$ integrates the isotopic signal of all PON consumed by the foraminifera over their lifetime (noting that while the turnover time for foraminifer tissue is unknown, it must be shorter than for the shell). The foraminifera chosen for isotope analysis in this study were adults, and the majority (all except potentially *G. siphonifera*; Bijma et al., 1998, Jonkers et al., 2015) reproduce on monthly or longer timescales, such that their FT-$\delta^{15}N$ likely integrates over weeks to months. Thus, the suspended PON sampled in the eddy is unlikely to reflect that consumed by the foraminifera during the period over which they generated the FT-$\delta^{15}N$ that we measured.

The discrepancy between the $\delta^{15}N$ trends evident in the nitrate and PON additionally illustrates the weakness in assuming that the isotopic signal of PON is solely generated through nitrate assimilation. While our sampling took place near the start of the nitrate resupply period in the Cape Basin (Fig. 3), the very deep eddy mixed layers (~250 m), would have caused severe light limitation of phytoplankton (Wallschuss et al., 2022); this, combined with the fact that nitrate is energetically expensive to assimilate (Dortch, 1990), likely led to limited consumption of newly-supplied nitrate near the time of our study. Indeed, direct measurements of N uptake in E1 indicate that phytoplankton were assimilating near-exclusively recycled N (Wallschuss et al., 2022). We conclude that discrepancies in the spatial $\delta^{15}N$ trends of contemporaneously sampled suspended

PON and foraminifera are not unexpected in highly variable environments given the different turnover times of these two N pools.

While the $\delta^{15}N$ of suspended PON does not align with the trends observed in the $\delta^{15}N_{NO3}$ and FT-$\delta^{15}N$, the bulk zooplankton $\delta^{15}N$ does (Fig. 7). It is thus possible that the zooplankton biomass (particularly in the 250 – 500 μm range, which had an N concentration 3-4 times that of the >0.3 μm suspended PON) more accurately represents the diet of the foraminifera. Not only are foraminifera known to consume other zooplankton in addition to PON (Bé and Hutson, 1977; Hemleben et al., 1989), but the zooplankton biomass integration time would have been more similar to that of the foraminifera (Montoya et al., 2002; Loick-Wilde et al., 2016). As such, the measured bulk zooplankton $\delta^{15}N$, which was ~2‰ lower in the eddy than the Atlantic, may better approximate the $\delta^{15}N$ of the organic matter consumed by foraminifera (Fig. S3).

4.4 Potential for reconstruction of past Agulhas leakage from foraminifer-bound $\delta^{15}N$

Our data show that foraminifera in Agulhas eddies retain the distinct $\delta^{15}N$ of Agulhas thermocline nitrate, which could be leveraged to trace Indo-Atlantic exchange through past climate transitions. Previous palaeoclimate studies have suggested that glacial-to-interglacial transitions were associated with increased leakage of Indian Ocean waters into the South Atlantic, which would have increased the salinity of waters returning to the North Atlantic, thus enhancing NADW subduction and strengthening the AMOC (e.g., Peeters et al., 2004; Franzese et al., 2006; Ballalai et al., 2019; Simon et al., 2020). Studies of fossil foraminifera collected in sediment cores from the western continental shelf of South Africa reveal a higher abundance of (sub)tropical species (i.e., Agulhas leakage fauna) during glacial terminations, consistent with an increase in the strength of Agulhas leakage at this time (Peeters et al., 2004; Caley et al., 2014). From our FT-$\delta^{15}N$ results and the strong correlation of FT-$\delta^{15}N$ to shell-bound $\delta^{15}N$ observed here and elsewhere (Fig. 8a; Ren et al., 2012; Smart et al., 2018, 2020), we would expect these glacial-interglacial transitions to also be characterized by comparatively low foraminifer-bound $\delta^{15}N$. In line with this expectation, anomalously low foraminifer-bound $\delta^{15}N$ values in Southern Ocean (~41°S) sediments from a "super interglacial" (Marine Isotope Stage 31, ~ 1070 ka) were recently hypothesized to reflect increased reliance on Agulhas-sourced N relative to Southern Ocean nitrate (Marcks et al., 2023).

Our samples were collected from a relatively mature Agulhas eddy and yet the isotopic influence of Agulhas nitrate was still apparent in the FT-$\delta^{15}N$. This observation suggests that the foraminifera-$\delta^{15}N$ proxy has the potential to provide an annually-integrated view of leakage, as it is independent of species assemblage, which shifts seasonally (Lončarić, 2006). Furthermore, foraminifer-bound $\delta^{15}N$ raises the possibility of extending Agulhas leakage reconstructions beyond the Retroflection region and into the offshore South Atlantic where Agulhas leakage fauna (e.g., *G. ruber, G. menardii, T. sacculifer*) no longer dominate surface waters due to cooling during eddy decay (Lončarić, 2006).

One caveat to these ideas is that the foraminifer-$\delta^{15}N$ leakage proxy relies on the $\delta^{15}N$ of Agulhas nitrate being distinct from that of the Cape Basin thermocline, as is the case today. Since Agulhas nitrate is low in $\delta^{15}N$ because of N_2 fixation, a past decrease in N_2 fixation in the southwest Indian Ocean would presumably lead to higher-$\delta^{15}N$ nitrate in the Agulhas Current, which would be passed on to the upper-ocean ecosystem, including the foraminifera. Similarly, a past increase in N_2 fixation in the South Atlantic, which today hosts negligible rates of this process (Moore et al.,

2009; Sohm et al., 2011), could have lowered the $\delta^{15}N$ of thermocline nitrate in the Cape Basin, weakening the $\delta^{15}N$ difference between Agulhas leakage and the surrounding Atlantic. An additional consideration is that we only have data from winter. At higher latitudes (e.g., in the southern Subantarctic/Polar Frontal Zone), winter is typically much less productive than summer, with lower total mass and foraminifera fluxes to the seafloor (Honjo et al., 2000; King & Howard, 2003), implying that winter N isotope signals may contribute minimally to the foraminifera-bound $\delta^{15}N$ record (Smart et al., 2020). However, in the lower latitudes (i.e., near the Subtropical Front and beyond), the flux to the seafloor is dominant (Nodder & Northcote, 2001; King & Howard, 2001) and in more oligotrophic waters, winter can even constitute a secondary peak in biomass production (e.g., Conte et al., 2001). Furthermore, several foraminifera species, such as the three *Globorotalia* species that dominated our collections, are more abundant in winter and spring than in summer. We therefore expect the distinctively low $\delta^{15}N$ of Agulhas leakage to be resolvable in seafloor sediments in the Cape Basin, at the very least in these more winter-typical species.

5 Conclusions

We compared the isotope ratios of nitrate, PON, bulk zooplankton, and foraminifera in an anticyclonic Agulhas eddy to those measured in the surrounding southeast Atlantic. We attribute the low $\delta^{15}N$ of the N in an anticyclonic Agulhas eddy to the retention of Agulhas-sourced nitrate, which is low in $\delta^{15}N$ (and Δ(15-18)) because of N_2 fixation in the southwest Indian Ocean (Harms et al., 2019; Marshall et al., 2023). This low $\delta^{15}N$ signal is retained by in-eddy foraminifera and other zooplankton even after the $\delta^{15}N$ of eddy mixed-layer nitrate is raised by phytoplankton nitrate assimilation and mixing with Cape Basin nitrate. Differences in the magnitude of the Atlantic-eddy $\delta^{15}N$ offset in mixed-layer nitrate, PON, bulk zooplankton, and foraminifera can be explained by the different integration times of these N pools. For instance, foraminifera and zooplankton assemblages inhabiting Agulhas eddies appear to retain the low $\delta^{15}N$ of Agulhas nitrate for several months, despite ongoing exchange with the surrounding Cape Basin and changes in the dominant foraminifer species. These findings are of particular relevance for tracking Agulhas leakage some distance from the Retroflection region.

Our data add to a growing body of work showing a strong (near 1:1) correlation between tissue- and shell-bound foraminifer $\delta^{15}N$ and confirm previous assertions that foraminifer-bound $\delta^{15}N$ is a faithful recorder of the $\delta^{15}N$ of the low-latitude subsurface nitrate supply (Ren et al., 2012; Smart et al., 2018). However, our observations differ from previous findings in that it is the deep-dwelling, non-symbiont-hosting foraminifer species rather than the shallow-dwelling, dinoflagellate-bearers that most closely match the $\delta^{15}N$ of thermocline nitrate, at least during winter when our sampling occurred.

Future investigations into spring and summer N dynamics in the Cape Basin would be useful for assessing the relationships among foraminifer $\delta^{15}N$, species assemblage, and shallow thermocline nitrate, as well as for determining the relative importance of seasonal fluxes (and consequently, the dominant $\delta^{15}N$ signals) reaching the sea floor (Smart et al., 2020). Additionally, PON and foraminifer isotope measurements in the Agulhas Current region (i.e., prior to the formation of eddies) would provide important end-member information that would assist in interpreting Agulhas eddy N isotope dynamics, as would observations from newly-formed Agulhas eddies. Comparing such data with the results of the present study would also allow us to disentangle

imported signals from *in situ* eddy processes that may alter nitrate and particle $\delta^{15}N$, such as in-eddy N_2 fixation and ammonium recycling that could have contributed to the low FT-$\delta^{15}N$ measured in the mature Agulhas eddy.

Acknowledgments

We are grateful to the Captain and crew of the R/V *S.A. Agulhas II* for their efforts during both the 2015 and 2017 SAMBA cruises, and would like to thank Chief Scientists I. Ansorge and M. van den Berg, as well as the South African Department of Forestry, Fisheries and Environment: Oceans and Coasts for providing the nets used during the 2017 voyage. We are also grateful to B. Hinnenberg, J. Luyt, I. Newton, S. Oleynik, R. Roman, F. Rubach and R. Schiebel for laboratory and technical expertise, H. Forrer, P. Kemeny and K. Spence, for help with sampling, and J. Magner for assistance with Figure 9. This work was supported by the South African Department of Science and Innovation (DSI) through their SEAmester programme (seamester.co.za), the South African National Research Foundation through grants 129320 and 116142 to SEF and grants 112379 and 121126 to RG, the University of Cape Town through a VC Future Leaders 2030 award and Research Committee Equipment grant to SEF, and by the Royal Society/African Academy of Sciences through a FLAIR Fellowship to SEF. The 2017 SAMBA nitrate and foraminifer nitrogen isotope analyses were supported by the Max Planck Society (MPG). The authors also acknowledge the DSI's Biogeochemistry Research Infrastructure Platform (BIOGRIP; www.biogrip.ac.za).

Data Availability

Nitrate isotope data for SAMBA 2017 can be found online at https://doi.org/10.5281/zenodo.7648606, whilst data for SAMBA 2015 is published by Marconi et al. (2017). Existing nitrate isotope data from the Agulhas Current (2015) can be found at https://doi.org/10.5281/zenodo.7628608. Foraminifera, zooplankton and PON data can be found at https://doi.org/10.5281/zenodo.10656959.

References

Altabet, M. A. (1988). Variations in nitrogen isotopic composition between sinking and suspended particles: implications for nitrogen cycling and particle transformation in the open ocean. *Deep Sea Research Part A, Oceanographic Research Papers*, *35*(4), 535–554. https://doi.org/10.1016/0198-0149(88)90130-6

Altabet, M. A., & Francois, R. (1994). Sedimentary nitrogen isotopic ratio as a recorder for surface ocean nitrate utilization. *Global Biogeochemical Cycles*, *8*(1), 103–116.

Altabet, M. A., & Francois, R. (2001). Nitrogen isotope biogeochemistry of the Antarctic polar frontal zone at 170 °W. *Deep-Sea Research Part II: Topical Studies in Oceanography*, *48*(19-20), 4247–4273. https://doi.org/10.1016/S0967-0645(01)00088-1

Altabet, M. A., & McCarthy, J. J. (1985). Temporal and spatial variations in the natural abundance of 15N in PON from a warm-core ring. *Deep Sea Research Part A, Oceanographic Research Papers*, *32*(7), 755–772. https://doi.org/10.1016/0198-0149(85)90113-X

Anand, P., Elderfield, H., & Conte, M. H. (2003). Calibration of Mg/Ca thermometry in planktonic foraminifera from a sediment trap time series. *Paleoceanography*, *18*(2). https://doi.org/10.1029/2002pa000846

Arhan, M., Mercier, H., & Lutjeharms, J. R. E. (1999). The disparate evolution of three Agulhas rings in the South Atlantic Ocean. *Journal of Geophysical Research: Oceans*, *104*(C9), 20987–21005. https://doi.org/10.1029/1998JC900047

Auderset, A., Moretti, S., Taphorn, B., Ebner, P. R., Kast, E., Wang, X. T., … Martínez-García, A. (2022). Enhanced ocean oxygenation during Cenozoic warm periods. *Nature*, *609*(7925), 77–82. https://doi.org/10.1038/s41586-022-05017-0

Aumont, O., Ethé, C., Tagliabue, A., Bopp, L., & Gehlen, M. (2015). PISCES-v2: An ocean biogeochemical model for carbon and ecosystem studies. *Geoscientific Model Development*, *8*(8), 2465–2513. https://doi.org/10.5194/gmd-8-2465-2015

Ballalai, J. M., Santos, T. P., Lessa, D. O., Venancio, I. M., Chiessi, C. M., Johnstone, H. J. H., … Albuquerque, A. L. S. (2019). Tracking Spread of the Agulhas Leakage Into the Western South Atlantic and Its Northward Transmission During the Last Interglacial. *Paleoceanography and Paleoclimatology*, *34*(11), 1744–1760. https://doi.org/10.1029/2019PA003653

Ballegooyen, R. C. van, Gründlingh, M. L., & Lutjeharms, J. R. E. (1994). Eddy fluxes of heat and salt from the southwest Indian Ocean into the southeast Atlantic Ocean: A case study. *Journal of Geophysical Research*, *99*(94), 14053–14070.

Beal, L., De Ruijter, W. P. M., Biastoch, A., Zahn, R., Cronin, M., Hermes, J., … Zinke, J. (2011). On the role of the Agulhas system in ocean circulation and climate. *Nature*, *472*(7344), 429–436. https://doi.org/10.1038/nature09983

Bergh, E. & Compton, J. (2020). Quaternary foraminifera and mollusc assemblages on the southwestern Africa shelf. *Palaeontologia Electronica*, *23*(2):a27, 1-28. https://doi.org/10.26879/1018

Berger, W. H., & Wefer, G. (2002). On the reconstruction of upwelling history: Namibia upwelling in context. *Marine Geology*, *180*(1-4), 3–28. https://doi.org/10.1016/S0025-3227(01)00203-1

Bé, A. W. H., Hemleben, C., Anderson, O. R., & Spindler, M. (1979). Chamber Formation in Planktonic Foraminifera. *Micropaleontology*, *25*(3), 294. https://doi.org/10.2307/1485304

Bé, A. W. H., & Hutson, W. H. (1977). Ecology of Planktonic Foraminifera and Biogeographic Patterns of Life and Fossil Assemblages in the Indian Ocean. *Micropaleontology*, *23*(4), 369. https://doi.org/10.2307/1485406

Bé, A. W. H., & Tolderlund, D. S. (1971). Distribution and ecology of living planktonic foraminifera in surface waters of the Atlantic and Indian Oceans.

Bijma, J., Faber, W. W., & Hemleben, C. (1990). Temperature and salinity limits for growth and survival of some planktonic foraminifers in laboratory cultures. *Journal of Foraminiferal Research*, *20*(2), 95–116. https://doi.org/10.2113/gsjfr.20.2.95

Bird, C., LeKieffre, C., Jauffrais, T., Meibom, A., Geslin, E., Filipsson, H. L., … Fehrenbacher, J. S. (2020). Heterotrophic Foraminifera Capable of Inorganic Nitrogen Assimilation. *Frontiers in Microbiology*, *11*(December), 3076. https://doi.org/10.3389/fmicb.2020.604979

Boltovskoy, D. (1994). The sedimentary record of pelagic biogeography. *Progress in Oceanography*, *34*(2-3), 135–160. https://doi.org/10.1016/0079-6611(94)90006-X

Boshers, D. S., Granger, J., Tobias, C. R., Böhlke, J. K., & Smith, R. L. (2019). Constraining the Oxygen Isotopic Composition of Nitrate Produced by Nitrification. *Environmental Science and Technology*, *53*(3), 1206–1216. https://doi.org/10.1021/acs.est.8b03386

Böhlke, J. K., Mroczkowski, S. J., & Coplen, T. B. (2003). Oxygen isotopes in nitrate: New reference materials for 18O:17O:16O measurements and observations on nitrate-water equilibration. *Rapid Communications in Mass Spectrometry*, *17*(16), 1835–1846. https://doi.org/10.1002/rcm.1123

Braman, R. S., & Hendrix, S. A. (1989). Nanogram Nitrite and Nitrate Determination in Environmental and Biological Materials by Vanadium(III) Reduction with Chemiluminescence Detection. *Analytical Chemistry*, *61*(24), 2715–2718. https://doi.org/10.1021/ac00199a007

Browning, T. J., Achterberg, E. P., Rapp, I., Engel, A., Bertrand, E. M., Tagliabue, A., & Moore, C. M. (2017). Nutrient co-limitation at the boundary of an oceanic gyre. *Nature*, *551*(7679), 242–246. https://doi.org/10.1038/nature24063

Buchwald, C., & Casciotti, K. L. (2010). Oxygen isotopic fractionation and exchange during bacterial nitrite oxidation. *Limnology and Oceanography*, *55*(3), 1064–1074. https://doi.org/10.4319/lo.2010.55.3.1064

Buchwald, C., & Casciotti, K. L. (2013). Isotopic ratios of nitrite as tracers of the sources and age of oceanic nitrite. *Nature Geoscience*, *6*(4), 1–6. https://doi.org/10.1038/ngeo1745

Caley, T., Giraudeau, J., Malaizé, B., Rossignol, L., & Pierre, C. (2012). Agulhas leakage as a key process in the modes of Quaternary climate changes. *PNAS*, *109*(18), 6835–6839. https://doi.org/10.1073/pnas.1115545109

Caley, T., Kim, J. H., Malaizé, B., Giraudeau, J., Laepple, T., Caillon, N., … Sinninghe Damsté, J. S. (2011). High-latitude obliquity as a dominant forcing in the Agulhas current system. *Climate of the Past*, *7*(4), 1285–1296. https://doi.org/10.5194/cp-7-1285-2011

Caley, T., Peeters, F. J. C., Biastoch, A., Rossignol, L., & Sebille, E. V. (2014). Quantitative estimate of the paleo-Agulhas leakage. *Geophysical Research Letters*, *41*, 1238–1246. https://doi.org/10.1002/2014GL059278.Received

Campbell, E. C. (2016). Where three oceans meet: Nitrate isotope measurements from the South Atlantic along 34.5°S. Senior thesis. Princeton University. http://arks.princeton.edu/ark:/88435/dsp01j3860941p

Capone, D. G., Bronk, D. A., Mulholland, M. R., & Carpenter, E. J. (2008). *Nitrogen in the Marine Environment* (2nd edition, p. 1729). Elsevier.

Carpenter, E. J., Harvey, H. R., Brian, F., & Capone, D. G. (1997). Biogeochemical tracers of the marine cyanobacterium Trichodesmium. *Deep-Sea Research Part I: Oceanographic Research Papers*, *44*(1), 27–38. https://doi.org/10.1016/S0967-0637(96)00091-X

Casciotti, K. L., & McIlvin, M. R. (2007). Isotopic analyses of nitrate and nitrite from reference mixtures and application to Eastern Tropical North Pacific waters. *Marine Chemistry*, *107*(2), 184–201. https://doi.org/10.1016/j.marchem.2007.06.021

Casciotti, K. L., Sigman, D. M., Hastings, M. G., Bohlke, J. K., & Hilkert, a. (2002). Measurement of the oxygen isotopic composition of nitrate seawater and freshwater using the dentirifier method. *Anal. Chem.*, *74*(19), 4905–4912. https://doi.org/10.1021/ac020113w

Cetina-Heredia, P., Roughan, M., Van Sebille, E., Shane, K., Gary, B., Keating, S., & Brassington, G. B. (2019). Retention and leakage of water by mesoscale eddies in the East Australian Current system. *Journal of Geophysical Research: Oceans*, *124*(4), 2485–2500. https://doi.org/10.1029/2018JC014482

Chapman, M. R. (2010). Seasonal production patterns of planktonic foraminifera in the NE Atlantic Ocean: Implications for paleotemperature and hydrographic reconstructions. *Paleoceanography*, *25*(1). https://doi.org/10.1029/2008PA001708

Checkley, D. M., & Miller, C. A. (1989). Nitrogen isotope fractionation by oceanic zooplankton. *Deep Sea Research Part A, Oceanographic Research Papers*, *36*(10), 1449–1456. https://doi.org/10.1016/0198-0149(89)90050-2

Chelton, D. B., Schlax, M. G., & Samelson, R. M. (2011). Global observations of nonlinear mesoscale eddies. *Progress in Oceanography*, *91*(2), 167–216. https://doi.org/10.1016/j.pocean.2011.01.002

Chen, G., Yang, J., & Han, G. (2021). Remote Sensing of Environment Eddy morphology : Egg-like shape, overall spinning, and oceanographic implications. *Remote Sensing of Environment*, *257*(March 2020), 112348. https://doi.org/10.1016/j.rse.2021.112348

Cléroux, C., Cortijo, J., Duplessy, J., Zahn, R. (2007). Deep-dwelling foraminifera as thermocline temperature recorders. *Geochemistry, Geophysics, Geosystems*, *8*(4), 1–19. https://doi.org/10.1029/2006GC001474

Condie, S., & Condie, R. (2016). Retention of plankton within ocean eddies. *Global Ecology and Biogeography*, *25*(10), 1264–1277. https://doi.org/10.1111/geb.12485

Conte, M.H., Ralph, N. & Ross, E.H. (2001). Seasonal and interannual variability in deep ocean particle fluxes at the Oceanic Flux Program (OFP)/Bermuda Atlantic Time Series (BATS) site in the western Sargasso Sea near Bermuda. *Deep-Sea Research II*, 48, 1471–1505. https://doi.org/10.1016/S0967-0645(00)00150-8

Conway, T. M., John, S. G., & Lacan, F. (2016). Intercomparison of dissolved iron isotope profiles from reoccupation of three GEOTRACES stations in the Atlantic Ocean. *Marine Chemistry*, *183*, 50–61. https://doi.org/10.1016/j.marchem.2016.04.007

d'Ovidio, F., De Monte, S., Alvain, S., Dandonneau, Y., & Levy, M. (2010). Fluid dynamical niches of phytoplankton types. *Proceedings of the National Academy of Sciences*, *107*(43), 18366–18370. https://doi.org/10.1073/pnas.1004620107

De Ruijter, W. P. M., Biastoch, A., Drijfhout, S. S., Lutjeharms, J. R. E., Matano, R. P., Pichevin, T., … Weijer, W. (1999). Indian-Atlantic interocean exchange: Dynamics, estimation and impact. *Journal of Geophysical Research*, *104*(C9), 20885–20910. https://doi.org/10.1029/1998JC900099

Deman, F., Fonseca-Batista, D., Roukaerts, A., García-Ibáñez, M. I., Le Roy, E., Thilakarathne, E. P. D. N., … Fripiat, F. (2021). Nitrate Supply Routes and Impact of Internal Cycling in the North Atlantic Ocean Inferred From Nitrate Isotopic Composition. *Global Biogeochemical Cycles*, *35*(4), 1–15. https://doi.org/10.1029/2020GB006887

Deniro, M., & Epstein, S. (1978) Influence of diet on the distribution of carbon isotopes in animals. *Geochimica et Cosmochimica Acta*, *42*, 495–506. https://doi.org/10.1002/mop.25285

Deuser, W. G., Ross, E. H., Hemleben, C., & Spindler, M. (1981). Seasonal changes in species composition, numbers, mass, size, and isotopic composition of planktonic foraminifera settling into the deep Sargasso Sea. *Palaeogeography Palaeoclimatology Palaeoecology*, *33*, 103–127.

Deutsch, C., Sarmiento, J. L., Sigman, D. M., Gruber, N., & Dunne, J. P. (2007). Spatial coupling of nitrogen inputs and losses in the ocean. *Nature*, *445*(7124), 163–167. https://doi.org/10.1038/nature05392

Diamond, D. (1994). Lachat Instruments Inc. *QuikChem Method*, 31–115.

Donners, J., Drijfhout, S. S., & Hazeleger, W. (2005). Water mass transformation and subduction in the South Atlantic. *Journal of Physical Oceanography*, *35*(10), 1841–1860. https://doi.org/10.1175/JPO2782.1

Dortch, Q. (1990). The interaction between ammonium and nitrate uptake in phytoplankton. *Marine Ecology Progress Series*, *61*(1), 183–201.

Dufois, F., Hardman-Mountford, N. J., Greenwood, J., Richardson, A. J., Feng, M., & Matear, R. J. (2016). Anticyclonic eddies are more productive than cyclonic eddies in subtropical gyres because of winter mixing. *Science Advances*, *2*(5), 1–6. https://doi.org/10.1126/sciadv.1600282

Duncombe Rae, C. M. (1991). Agulhas retroflection rings in the South Atlantic Ocean: An overview. *South African Journal of Marine Science*, *11*(1), 327–344. https://doi.org/10.2989/025776191784287574

Eguchi, N. O., Ujiié, H., Kawahata, H., & Taira, A. (2003). Seasonal variations in planktonic foraminifera at three sediment traps in the Subarctic, Transition and Subtropical zones of the central North Pacific Ocean. *Marine Micropaleontology*, *48*(1-2), 149–163. https://doi.org/10.1016/S0377-8398(03)00020-3

Eppley, R. W., Renger, E. H., & Betzer, P. R. (1983). The residence time of particulate organic carbon in the surface layer of the ocean. *Deep Sea Research Part A, Oceanographic Research Papers*, *30*(3), 311–323. https://doi.org/10.1016/0198-0149(83)90013-4

Faber, W. W., Anderson, O. R., Lindsey, J. L., & Caron, D. A. (1988). Algal-foraminiferal symbiosis in the planktonic foraminifer Globigerinella aequilateralia; I, Occurrence and stability of two mutually exclusive chrysophyte endosymbionts and their ultrastructure. *Journal of Foraminiferal Research*, *18*(4), 334–343. https://doi.org/10.2113/gsjfr.18.4.334

Fasham, M. J. R., Ducklow, H. W., & McKelvie, S. M. (1990). A nitrogen-based model of plankton dynamics in the oceanic mixed layer. *Journal of Marine Research*, *48*(3), 591–639. https://doi.org/10.1357/002224090784984678

Fawcett, S. E., Lomas, M. W., Casey, J. R., Ward, B. B., & Sigman, D. M. (2011). Assimilation of upwelled nitrate by small eukaryotes in the Sargasso Sea. *Nature Geoscience*, *4*(10), 717–722. https://doi.org/10.1038/ngeo1265

Fawcett, S. E., Lomas, M. W., Ward, B. B., & Sigman, D. M. (2014). The counterintuitive effect of summer-to-fall mixed layer deepening on eukaryotic new production in the Sargasso Sea. *Global Biogeochemical Cycles*, *28*, 86–102. https://doi.org/10.1002/2013GB004579.Received

Fawcett, S. E., Ward, B. B., Lomas, M. W., & Sigman, D. M. (2015). Vertical decoupling of nitrate assimilation and nitrification in the Sargasso Sea. *Deep-Sea Research Part I: Oceanographic Research Papers*, *103*, 64–72. https://doi.org/10.1016/j.dsr.2015.05.004

Feldmeijer, W., Metcalfe, B., Brummer, G. J. A., & Ganssen, G. M. (2015). Reconstructing the depth of the permanent thermocline through the morphology and geochemistry of the deep dwelling planktonic foraminifer Globorotalia truncatulinoides. *Paleoceanography*, *30*(1), 1–22. https://doi.org/10.1002/2014PA002687

Ferreira, M. L. de C., & Kerr, R. (2017). Source water distribution and quantification of North Atlantic Deep Water and Antarctic Bottom Water in the Atlantic Ocean. *Progress in Oceanography*, *153*, 66–83. https://doi.org/10.1016/j.pocean.2017.04.003

Flynn, R. F., Granger, J., Veitch, J. A., Siedlecki, S., Burger, J. M., Pillay, K., & Fawcett, S. E. (2020). On-Shelf Nutrient Trapping Enhances the Fertility of the Southern Benguela Upwelling System. *Journal of Geophysical Research: Oceans*, *125*(6), 1–24. https://doi.org/10.1029/2019JC015948

Fong, A. A., Karl, D. M., Lukas, R., Letelier, R. M., Zehr, J. P., & Church, M. J. (2008). Nitrogen fixation in an anticyclonic eddy in the oligotrophic North Pacific Ocean. *ISME Journal*, *2*(6), 663–676. https://doi.org/10.1038/ismej.2008.22

Franzese, A. M., Hemming, S. R., Goldstein, S. L., & Anderson, R. F. (2006). Reduced Agulhas Leakage during the Last Glacial Maximum inferred from an integrated provenance and flux study. *Earth and Planetary Science Letters*, *250*, 72–88. https://doi.org/10.1016/j.epsl.2006.07.002

Friedrich, O., Schiebel, R., Wilson, P. A., Weldeab, S., Beer, C. J., Cooper, M. J., & Fiebig, J. (2012). Influence of test size, water depth, and ecology on Mg/Ca, Sr/Ca, $\delta^{18}O$ and $\delta^{13}C$ in nine modern species of planktic foraminifers. *Earth and Planetary Science Letters*, *319-320*, 133–145. https://doi.org/10.1016/j.epsl.2011.12.002

Froyland, G., Horenkamp, C., Rossi, V., & Sebille, E. van. (2015). Studying an Agulhas ring's long-term pathway and decay with finite-time coherent sets. *Chaos*, *25*(8), 083119. https://doi.org/10.1063/1.4927830

Garcia, H. E., Weathers, K., Paver, C. R., Smolyar, I., Boyer, T. P., Locarnini, R. A., … Reagan, J. R. (2019). World Ocean Atlas 2018, Volume 4: Dissolved Inorganic Nutrients (phosphate, nitrate and nitrate+nitrite, silicate). In A. Mishnov Technical Editor (Ed.), *NOAA atlas NESDIS 84*, 35.

Garzoli, S. L., & Gordon, A. L. (1996). Origins and variablity of the Benguela Current. *Journal of Geophysical Research*, *101*(95), 897–906.

Garzoli, S. L., & Matano, R. P. (2011). The South Atlantic and the Atlantic Meridional Overturning Circulation. *Deep-Sea Research Part II: Topical Studies in Oceanography*, *58*(17-18), 1837–1847. https://doi.org/10.1016/j.dsr2.2010.10.063

Gastrich, M. (1987). Ultrastructure of a new intracellular symbiotic alga found within planktonic foraminifera. *Journal of Phycology*, *25*, 623–632.

Gonfiantini, R., Stichler, W., & Rozanski, K. (1993). Standards and intercomparison materials distributed by the International Atomic Energy Agency for stable isotope measurements. *Standards and Intercomparison Materials Distributed by the International Atomic Energy Agency for Stable Isotope Measurements*, (No. IAEA-TECDOC–825).

Goni, G. J., Garzoli, S. L., Roubicek, A. J., Olson, D. B., & Brown, O. B. (1997). Agulhas ring dynamics from TOPEX/POSEIDON satellite altimeter data. *Journal of Marine Research*, *55*(5), 861–883. https://doi.org/10.1357/0022240973224175

Gordon, A. L. (1986). Interocean exchange of thermocline water. *Journal of Geophysical Research*, *91*(C4), 5037. https://doi.org/10.1029/jc091ic04p05037

Gordon, A. L., & Haxby, W. F. (1990). Agulhas eddies invade the south Atlantic: Evidence From Geosat altimeter and shipboard conductivity-temperature-depth survey. *Journal of Geophysical Research*, *95*(C3), 3117. https://doi.org/10.1029/JC095iC03p03117

Gordon, A. L., & Huber, B. A. (1990). Southern ocean winter mixed layer. *Journal of Geophysical Research*, *95*(C7), 11655. https://doi.org/10.1029/jc095ic07p11655

Gordon, A. L., Lutjeharms, J. R. E., & Gründlingh, M. L. (1987). Stratification and circulation at the Agulhas Retroflection. *Deep Sea Research Part A, Oceanographic Research Papers*, *34*(4), 565–599. https://doi.org/10.1016/0198-0149(87)90006-9

Gordon, A. L., Weiss, R., Smethie, W. M., & Warner, M. J. (1992). Thermocline and Intermediate Water Communication Between the South Atlantic and Indian Oceans. *Journal of Geophysical …*, *97*, 7223–7240. Retrieved from http://www.ldeo.columbia.edu/~agordon/publications/Gordon_etal_1992_JGR.pdf

Granger, J., & Sigman, D. M. (2009). Removal of nitrite with sulfamic acid for nitrate N and O isotope analysis with the denitrifier method. *Rapid Communications in Mass Spectrometry*, *23*, 3753–3762. https://doi.org/10.1002/rcm

Granger, J., Sigman, D. M., Needoba, J. A., & Harrison, P. J. (2004). Coupled nitrogen and oxygen isotope fractionation of nitrate during assimilation by cultures of marine phytoplankton. *Limnology and Oceanography*, *49*(5), 1763–1773. https://doi.org/10.4319/lo.2004.49.5.1763

Granger, J., Sigman, D. M., Rohde, M. M., Maldonado, M. T., & Tortell, P. D. (2010). N and O isotope effects during nitrate assimilation by unicellular prokaryotic and eukaryotic plankton cultures. *Geochimica Et Cosmochimica Acta*, *74*(3), 1030–1040. https://doi.org/10.1016/j.gca.2009.10.044

Grasshoff, K. (1976). *Methods of Seawater Analysis* (2nd ed.). Verlag Chemie.

Haas, S., Rakshit, S., Kalvelage, T., Buchwald, C., Algar, C., Wallace, D.(2022). Characterization of nitrogen isotope fractionation during nitrification based on a coastal time series. *Limnology and Oceanography*, *9999*, 1–18. https://doi.org/10.1002/lno.12161

Harms, N. C., Lahajnar, N., Gaye, B., Rixen, T., Dähnke, K., Ankele, M., … Emeis, K. C. (2019). Nutrient distribution and nitrogen and oxygen isotopic composition of nitrate in water masses of the subtropical southern Indian Ocean. *Biogeosciences*, *16*(13), 2715–2732. https://doi.org/10.5194/bg-16-2715-2019

Hecht, A. D. (1976). An ecologic model for test size variation in Recent planktonic foraminifera; applications to the fossil record. *The Journal of Foraminiferal Research*, *6*(4), 295–311. https://doi.org/10.2113/gsjfr.6.4.295

Hemleben, C., Bé, A. W. H., Anderson, O. R., & Tunitivate, S. (1977). Test morphology, organic layers and chamber formation of the planktonic foraminifer Globorotalia menardii (D'Orbigny). *Journal of Foraminiferal Research*, *7*(1), 1–25.

Hemleben, C., Spindler, M., & Anderson, O. R. (1989). *Modern Planktonic Foraminifera.* (1st ed., 1–363). New York: Springer-Verlag. https://doi.org/10.2113/gsjfr.20.1.90

Hemleben, C., Spindler, M., Breitinger, I., & Deuser, W. G. (1985). Field and laboratory studies on the ontogeny and ecology of some globorotaliid species from the Sargasso Sea off Bermuda. *Journal of Foraminiferal Research*, *15*(4), 254–272. https://doi.org/10.2113/gsjfr.15.4.254

Henehan, M. J., Rae, J. W. B., Foster, G. L., Erez, J., Prentice, K. C., Kucera, M., … Elliott, T. (2013). Calibration of the boron isotope proxy in the planktonic foraminifera Globigerinoides ruber for use in palaeo-CO_2 reconstruction. *Earth and Planetary Science Letters*, *364*, 111–122. https://doi.org/10.1016/j.epsl.2012.12.029

Hermes, J., Reason, C. J. C., & Lutjeharms, J. R. E. (2007). Modeling the variability of the greater Agulhas Current system. *Journal of Climate*, *20*(13), 3131–3146. https://doi.org/10.1175/JCLI4154.1

Hoering, T. C., & Ford, H. T. (1960). The Isotope Effect in the Fixation of Nitrogen by Azotobacter. *J. Am Chem Soc.*, *82*, 376–378.

Holl, C. M., Waite, A. M., Pesant, S., Thompson, P. A., & Montoya, J. P. (2007). Unicellular diazotrophy as a source of nitrogen to Leeuwin Current coastal eddies. *Deep-Sea Research Part II: Topical Studies in Oceanography*, *54*(8-10), 1045–1054. https://doi.org/10.1016/j.dsr2.2007.02.002

Holmes, E., Lavik, G., Fischer, G., Segl, M., Ruhland, G., & Wefer, G. (2002). Seasonal variability of $\delta^{15}N$ in sinking particles in the Benguela Upwelling region. *Deep-Sea Res.(I Oceanogr.Res.Pap.)*, *49*(2), 377–394.

Hönisch, B., Fish, C. R., Phelps, S. R., Haynes, L. L., Dyez, K. A., Holland, K., … Goes, J. I. (2021). Symbiont Photosynthesis and Its Effect on Boron Proxies in Planktic Foraminifera. *Paleoceanography and Paleoclimatology*, *36*(10), 1–22. https://doi.org/10.1029/2020PA004022

Hönisch, B., & Hemming, N. G. (2004). Ground-truthing the boron isotope-paleo-pH proxy in planktonic foraminifera shells: Partial dissolution and shell size effects. *Paleoceanography*, *19*(4), 1–13. https://doi.org/10.1029/2004PA001026

Honjo, S., Francois, R., Manganini, S., Dymond, J. and Collier, R. (2000). Particle fluxes to the interior of the Southern Ocean in the Western Pacific sector along 170°W. *Deep Sea Research II*, *47*(15), 3521–3548. https://doi.org/10.1016/S0967-0645(00)00077-1

Jonkers, L., & Kučera, M. (2015). Global analysis of seasonality in the shell flux of extant planktonic Foraminifera. *Biogeosciences*, *12*(7), 2207–2226. https://doi.org/10.5194/bg-12-2207-2015

Jonkers, Lukas, & Kučera, M. (2017). Quantifying the effect of seasonal and vertical habitat tracking on planktonic foraminifera proxies. *Climate of the Past*, *13*(6), 573–586. https://doi.org/10.5194/cp-13-573-2017

Kast, E. R., Stolper, D. A., Auderset, A., Higgins, J. A., Ren, H., Wang, X. T., … Stopler, D. (2019). Nitrogen isotope evidence for expanded ocean suboxia in the early Cenozoic. *Science*, *364*(6438), 386–389. https://doi.org/10.1126/science.aau5784

Kemle-von Mücke, S. and Oberhänsli, H.: The distribution of living planktic foraminifera in relation to southeast Atlantic oceanography, in: Use of Proxies in Paleoceanography, Springer Berlin Heidelberg, 91–115, (1999). https://doi.org/10.1007/978-3-642-58646-0_3

King, K., & Hare, P. E. (1972). Amino Acid Composition of the Test as a Taxonomic Character for Living and Fossil Planktonic Foraminifera. *Micropaleontology*, *18*(3), 285. https://doi.org/10.2307/1485009

King, A.L. and Howard, W.R. (2001). Seasonality of foraminiferal flux in sediment traps at Chatham Rise, SW Pacific: implications for paleotemperature estimates. *Deep Sea Research I*, *48*(7), 1687–1708. https://doi.org/10.1016/S0967-0637(00)00106-0

King, A.L. and Howard, W.R. (2003). Planktonic foraminiferal flux seasonality in Subantarctic sediment traps: A test for paleoclimate reconstructions. *Paleoceanography*, *18*(1). https://doi.org/10.1029/2002PA000839

Knapp, A. N., DiFiore, P. J., Deutsch, C., Sigman, D. M., & Lipschultz, F. (2008). Nitrate isotopic composition between Bermuda and Puerto Rico: Implications for N_2 fixation in the Atlantic Ocean. *Global Biogeochemical Cycles*, *22*(3), 1–14. https://doi.org/10.1029/2007GB003107

Knapp, A. N., Sigman, D. M., & Lipschultz, F. (2005). N isotopic composition of dissolved organic nitrogen and nitrate at the Bermuda Atlantic Time-series study site. *Global Biogeochemical Cycles*, *19*(1), 1–15. https://doi.org/10.1029/2004GB002320

Knorr, G., & Lohmann, G. (2003). Southern Ocean origin for the resumption of Atlantic thermohaline circulation during deglaciation. *Letters to Nature*, *424*(July), 532–536. https://doi.org/10.1038/nature01856.1.

Kretschmer, K., Jonkers, L., Kucera, M., & Schulz, M. (2018). Modeling seasonal and vertical habitats of planktonic foraminifera on a global scale. *Biogeosciences*, *15*(14), 4405–4429. https://doi.org/10.5194/bg-15-4405-2018

Landolfi, A., Kähler, P., Koeve, W., & Oschlies, A. (2018). Global marine N_2 fixation estimates: From observations to models. *Frontiers in Microbiology*, *9*(SEP), 1–8. https://doi.org/10.3389/fmicb.2018.02112

Lea, D. J., Mirouze, I., Martin, M. J., King, R. R., Hines, A., Walters, D., & Thurlow, M. (2018). GLOBAL_ANALYSISFORECAST_PHY_CPL_001_015. E.U. Copernicus Marine Service Information.

Lekieffre, C., Spero, H. J., Fehrenbacher, J. S., Russell, A. D., Ren, H., Geslin, E., & Meibom, A. (2020). Ammonium is the preferred source of nitrogen for planktonic foraminifer and their dinoflagellate symbionts: N recycling in a symbiotic foraminifer. *Proceedings of the Royal Society B: Biological Sciences*, *287*(1929), 1–10. https://doi.org/10.1098/rspb.2020.0620rspb20200620

Lessa, D., Morard, R., Jonkers, L., Venancio, I. M., Reuter, R., Baumeister, A., … Kucera, M. (2020). Distribution of planktonic foraminifera in the subtropical South Atlantic: depth hierarchy of controlling factors. *Biogeosciences*, *17*(16), 4313–4342. https://doi.org/10.5194/bg-17-4313-2020

Li, D. W., Xiang, R., Wu, Q., & Kao, S. J. (2019). Planktic foraminifera-bound organic nitrogen isotopic composition in contemporary water column and sediment trap. *Deep-Sea Research Part I*, *143*, 28–34. https://doi.org/10.1016/j.dsr.2018.12.003

Liu, Kon-Kee, Kao, Shuh-Ji, Wen, Liang-Saw, Chen, Kuan-Lun. (2007). Carbon and nitrogen isotopic compositions of particulate organic matter and biogeochemical processes in the eutrophic Danshuei Estuary in northern Taiwan. Science Direct. 382(2007), 104–120. https://doi:10.1016/j.scitotenv.2007.04.019

Liu, J., Zhou, L., Li, J., Lin, Y., Ke, Z., Zhao, C., … Tan, Y. (2020). Effect of mesoscale eddies on diazotroph community structure and nitrogen fixation rates in the South China Sea. *Regional Studies in Marine Science*, *35*, 1–14. https://doi.org/10.1016/j.rsma.2020.101106

Locarini, R. A., Mishonov, A. V., Antonov, J. I., Boyer, T. P., Garcia, H. E., Baranova, O. K., … Seidov, D. (2013). *World Ocean Atlas 2013, Volume 1: Temperature*. (S. Levitus & A. Mishanov, Eds.) (p. 40). NOAA Atlas NESDIS 73.

Lohmann, G. P., & Schweitzer, P. N. (1989). Globorotalia truncatulinoides' growth and chemistry as probes of the past thermocline: 1. Shell size. *Palaeoceanography*, *5*(1), 55–75.

Loick-Wilde, N., Weber, S. C., Conroy, B. J., Capone, D. G., Coles, V. J., Medeiros, P. M., … Montoya, J. P. (2016). Nitrogen sources and net growth efficiency of zooplankton in three Amazon River plume food webs. *Limnology and Oceanography*, *61*(2), 460–481. https://doi.org/10.1002/lno.10227

Lombard, F., Labeyrie, L., Michel, E., Bopp, L., Cortijo, E., Retailleau, S., … Jorissen, F. (2011). Modelling planktic foraminifer growth and distribution using an ecophysiological multi-species approach. *Biogeosciences*, *8*(4), 853–873. https://doi.org/10.5194/bg-8-853-2011

Lončarić, N. (2006). Planktic foraminiferal content in a mature Agulhas eddy from the SE Atlantic: Any influence on foraminiferal export fluxes? *Geologia Croatica*, *59*(1), 41–50.

Löscher, C. R., Bourbonnais, A., Dekaezemacker, J., Charoenpong, C. N., Altabet, M. A., Bange, H. W., … Schmitz, R. (2016). N_2 fixation in eddies of the eastern tropical South Pacific Ocean. *Biogeosciences*, *13*(10), 2889–2899. https://doi.org/10.5194/bg-13-2889-2016

Luo, Y. W., Doney, S. C., Anderson, L. A., Benavides, M., Berman-Frank, I., Bode, A., … Zehr, J. P. (2012). Database of diazotrophs in global ocean: Abundance, biomass and nitrogen fixation rates. *Earth System Science Data*, *4*(1), 47–73. https://doi.org/10.5194/essd-4-47-2012

Lutjeharms, J. R. E., & Cooper, J. (1996). Interbasin leakage through Agulhas current filaments. *Deep-Sea Research*, *43*(2), 213–238.

Lutjeharms, J. R. E., & Gordon, A. L. (1987). Shedding of an Agulhas ring observed at sea. *Nature*, *325*, 138–140.

Lutjeharms, J. R. E., & Valentine, H. R. (1984). Southern ocean thermal fronts south of Africa. *Deep Sea Research Part A. Oceanographic Research Papers*, *31*(12), 1461–1475. https://doi.org/10.1016/0198-0149(84)90082-7

Marconi, D., Weigand, M. A., & Sigman, D. M. (2019). Nitrate isotopic gradients in the North Atlantic Ocean and the nitrogen isotopic composition of sinking organic matter. *Deep-Sea Research Part I: Oceanographic Research Papers*, *145*, 109–124. https://doi.org/10.1016/j.dsr.2019.01.010

Marcks, B. A., Dos Santos, T. P., Lessa, D. V. O., Cartagena-Sierra, A., Berke, M. A., Starr, A., et al. (2023). Glacial Southern Ocean expansion recorded in foraminifera-bound nitrogen isotopes from the Agulhas Plateau during the mid-Pleistocene transition. *Paleoceanography and Paleoclimatology*, 38, e2022PA004482. https://doi. org/10.1029/2022PA004482

Mariotti, A., A, Germon, J. C., Hubert, P., Kaiser, P., Letolle, R., & Tardieux, A. (1981). Experimental determination of nitrogen kinetic isotope fractionation: some principles: illustration for the denitrification and nitrification processes. *Plant and Soil*, *62*(3), 413–430.

Marshall, T., Granger, J., Casciotti, K. Dähnke, K., Emeis, K., Marconi, D., McIlvin, M. R., Noble, A. E., Saito, M. A., Sigman, D., Fawcett, S. E. (2022). The Angola Gyre is a hotspot of dinitrogen fixation in the South Atlantic Ocean. *Communications Earth and Environment*, *3*(151), 1–10. https://doi.org/10.1038/s43247-022-00474-x

Marshall, T. A., Sigman, D. M., Beal, L. M., Foreman, A., Martínez-García, A., Blain, S., … Fawcett, S. E. (2023). The Agulhas Current Transports Signals of Local and Remote Indian Ocean Nitrogen Cycling. *Journal of Geophysical Research: Oceans*, *128*, 1–29. https://doi.org/10.1029/2022jc019413

Martin, B., Koppelmann, R., Harmer, A., and Plonus, R.-M. (2024) Possible transport pathway of diazotrophic Trichodesmium by Agulhas Leakage from the Indian into the Atlantic Ocean. *Sci Rep*, *14*(1), 2906, https://doi.org/10.1038/s41598-024-53297-5.

Martínez-García, A., Jung, J., Ai, X. E., Sigman, D. M., Auderset, A., Duprey, N. N., … Wald, T. (2022). Laboratory Assessment of the Impact of Chemical Oxidation, Mineral Dissolution, and Heating on the Nitrogen Isotopic Composition of Fossil-Bound Organic Matter. *Geochemistry, Geophysics, Geosystems*, *23*(8), 1–23. https://doi.org/10.1029/2022GC010396

Martínez-García, A., Sigman, D. M., Ren, H., Anderson, R. F., Straub, M., Hodell, D. A., … Haug, G. H. (2014). Iron fertilization of the Subantarctic ocean during the last ice age. *Science (New York, N.Y.)*, *343*(6177), 1347–1350. https://doi.org/10.1126/science.1246848

Martínez-Méndez, G., Zahn, R., Hall, I. R., Peeters, F. J. C., Pena, L. D., Cacho, I., … Méndez, G. M. (2010). Contrasting multiproxy reconstructions of surface ocean hydrography in the Agulhas Corridor and implications for the Agulhas Leakage during the last 345,000 years. *Paleoceanography*, *25*, 1–12. https://doi.org/10.1029/2009PA001879

Meckler, A. N., Ren, H., Sigman, D. M., Gruber, N., Plessen, B., Schubert, C. J., & Haug, G. H. (2011). Deglacial nitrogen isotope changes in the Gulf of Mexico: Evidence from bulk sedimentary and foraminifera-bound nitrogen in Orca Basin sediments. *Paleoceanography*, *26*(4), 1–13. https://doi.org/10.1029/2011PA002156

Meilland, J., Schiebel, R., Lo Monaco, C., Sanchez, S., & Howa, H. (2018). Abundances and test weights of living planktic foraminifers across the Southwest Indian Ocean: Implications for carbon

fluxes. *Deep-Sea Research Part I: Oceanographic Research Papers*, *131*, 27–40. https://doi.org/10.1016/j.dsr.2017.11.004

Meilland, J., Siccha, M., Weinkauf, M. F. G., Jonkers, L., Morard, R., Baranowski, U., … Kucera, M. (2019). Highly replicated sampling reveals no diurnal vertical migration but stable species-specific vertical habitats in planktonic foraminifera. *Journal of Plankton Research*, *41*(2), 127–141. https://doi.org/10.1093/plankt/fbz002

Minagawa, M., & Wada, E. (1986). Nitrogen isotope ratios of red tide organisms in the East China Sea: A characterization of biological nitrogen fixation. *Marine Chemistry*, *19*(3), 245–259. https://doi.org/10.1016/0304-4203(86)90026-5

Mino, Y., Sukigara, C., Honda, M. C., Kawakami, H., Wakita, M., Sasaoka, K., … Saino, T. (2020). Seasonal and Interannual Variations in Nitrogen Availability and Particle Export in the Northwestern North Pacific Subtropical Gyre. *Journal of Geophysical Research: Oceans*, *125*(5), 1–18. https://doi.org/10.1029/2019JC015600

Mobius, J. (2013). Isotope fractionation during nitrogen remineralization (ammonification): Implications for nitrogen isotope biogeochemistry. *Geochimica Et Cosmochimica Acta*, *105*, 422–432. https://doi.org/10.1016/j.gca.2012.11.048

Mohtadi, M., Max, L., Hebbeln, D., Baumgart, A., Krück, N., & Jennerjahn, T. (2007). Modern environmental conditions recorded in surface sediment samples off W and SW Indonesia: Planktonic foraminifera and biogenic compounds analyses. *Marine Micropaleontology*, *65*(1-2), 96–112. https://doi.org/10.1016/j.marmicro.2007.06.004

Montoya, J. P., Horrigan, S. G., & McCarthy, J. J. (1990). Natural abundance in particulate nitrogen and zooplankton in the Chesapeake Bay. *Marine Ecology Progress Series. 65(1)*, 35–61. https:doi.org/10.3354/meps065035

Montoya, J. P., Carpenter, E. J., & Capone, D. G. (2002). Nitrogen fixation and nitrogen isotope abundance in zooplankton of the oligotrophic North Atlantic. *Limnology & Oceanography*, *47*(6), 1617–1628. https://doi.org/10.4319/lo.2002.47.6.1617

Moore, M. C., Mills, M. M., Achterberg, E. P., Geider, R. J., Laroche, J., Lucas, M. I., … Woodward, E. M. S. (2009). Large-scale distribution of Atlantic nitrogen fixation controlled by iron availability. *Nature Geoscience*, *2*(12), 867–871. https://doi.org/10.1038/ngeo667

Moretti, S., Auderset, A., Deutsch, C., Schmitz, R., Gerber, L., Thomas, E., Luciani, V., Petrizzo, M.R., Schiebel, R., Tripati, A., Sexton, P., Norris, R., D'Onofrio, R., Zachos, J., Sigman, D.M., Haug, G.H. and Martínez-García, A. (2024). Oxygen rise in the tropical upper ocean during the Paleocene-Eocene Thermal Maximum. *Science*, 383(6684), 727–731. https://doi.org/10.1126/science.adh4893.

Morris, T., Hermes, J., Beal, L., Du Plessis, M., Rae, C. M. D., Gulekana, M., … Ansorge, I. J. (2017). The importance of monitoring the Greater Agulhas Current and its inter-ocean exchanges using large mooring arrays. *South African Journal of Science*, *113*(7-8), 1–7. https://doi.org/10.17159/sajs.2017/20160330

Moutin, T., & Prieur, L. (2012). Influence of anticyclonic eddies on the Biogeochemistry from the Oligotrophic to the Ultraoligotrophic Mediterranean (BOUM cruise). *Biogeosciences*, *9*(10), 3827–3855. https://doi.org/10.5194/bg-9-3827-2012

Nodder, S.D. & Northcote, L.C. (2001). Episodic particulate fluxes at southern temperate mid-latitudes (42–45°S) in the Subtropical Front region, east of New Zealand. *Deep Sea Research I*, *48*(3), 833–864. https://doi.org/10.1016/S0967-0637(00)00062-5

Nydahl, F. (1978). On the peroxodisulphate oxidation of total nitrogen in waters to nitrate. *Water Research Vol.*, *12*, 1123–1130.

Olson, D. B., Fine, R. A., & Gordon, A. L. (1992). Convective modifications of water masses in the Agulhas. *Deep Sea Research Part A. Oceanographic Research Papers*, *39*(March), S163–S181. https://doi.org/10.1016/s0198-0149(11)80010-5

Palter, J. B., Sarmiento, J. L., Gnanadesikan, A., Simeon, J., & Slater, R. D. (2010). Fueling export production: Nutrient return pathways from the deep ocean and their dependence on the Meridional Overturning Circulation. *Biogeosciences*, *7*(11), 3549–3568. https://doi.org/10.5194/bg-7-3549-2010

Pasquero, C. (2005). Differential eddy diffusion of biogeochemical tracers. *Geophysical Research Letters*, *32*(17), 1–4. https://doi.org/10.1029/2005GL023662

Paul, M., Van De Flierdt, T., Rehkämper, M., Khondoker, R., Weiss, D., Lohan, M. C., & Homoky, W. B. (2015). Tracing the Agulhas leakage with lead isotopes. *Geophysical Research Letters*, *42*(20), 8515–8521. https://doi.org/10.1002/2015GL065625

Peeters, F. J. C., Acheson, R., Brummer, G.-J. A., De Ruijter, W. P. M., Schneider, R., Ganssen, G. M., … Kroon, D. (2004). Vigorous exchange between the Indian and Atlantic oceans at the end of the past five glacial periods. *Nature*, *430*(7000), 661–665. https://doi.org/10.1038/nature02785

Peeters, F. J. C., & Brummer, G. J. A. (2002). The seasonal and vertical distribution of living planktic foraminifera in the NW Arabian Sea. *Geological Society Special Publication*, *195*, 463–497. https://doi.org/10.1144/GSL.SP.2002.195.01.26

Qi, H., Coplen, T. B., Geilmann, H., Brand, W. A., & Böhlke, J. K. (2003). Two new organic reference materials for δ^{13}C and δ^{15}N measurements and a new value for the δ 13C of NBS 22 oil. *Rapid Communications in Mass Spectrometry*, *17*(22), 2483–2487. https://doi.org/10.1002/rcm.1219

Raes, E. J., Thompson, P. A., McInnes, A. S., Nguyen, H. M., Hardman-Mountford, N. J., & Waite, A. M. (2015). Sources of new nitrogen in the Indian Ocean. *Global Biogeochemical Cycles*, *29*, 1283–1297. https://doi.org/10.1002/2015GB005194.Received

Rafter, P. A., Difiore, P. J., & Sigman, D. M. (2013). Coupled nitrate nitrogen and oxygen isotopes and organic matter remineralization in the Southern and Pacific Oceans. *Journal of Geophysical Research: Oceans*, *118*(10), 4781–4794. https://doi.org/10.1002/jgrc.20316

Rebotim, A., Voelker, A. H. L., Jonkers, L., Waniek, J. J., Meggers, H., Schiebel, R., … Kucera, M. (2017). Factors controlling the depth habitat of planktonic foraminifera in the subtropical eastern North Atlantic. *Biogeosciences*, *14*(4), 827–859. https://doi.org/10.5194/bg-14-827-2017

Ren, H., Sigman, D. M., Meckler, A. N., Plessen, B., Robinson, R. S., Rosenthal, Y., & Haug, G. H. (2009). Foraminiferal isotope evidence of reduced nitrogen fixation in the ice age Atlantic Ocean. *Science*, *323*(5911), 244–248. https://doi.org/10.1126/science.1165787

Ren, H., Sigman, D. M., Thunell, R. C., & Prokopenko, M. G. (2012). Nitrogen isotopic composition of planktonic foraminifera from the modern ocean and recent sediments. *Limnology and Oceanography*, *57*(4), 1011–1024. https://doi.org/DOI 10.4319/lo.2012.57.4.1011

Ren, H., Studer, A. S., Serno, S., Sigman, D. M., Winckler, G., Anderson, R. F., … Haug, G. H. (2015). Glacial-to-interglacial changes in nitrate supply and consumption in the subarctic North Pacific from microfossil-bound N isotopes at two trophic levels. *Paleoceanography*, *30*(9), 1217–1232. https://doi.org/10.1002/2014PA002765

Rintoul, S. R. (1991). South Atlantic interbasin exchange. *Journal of Geophysical Research: Oceans*, *96*(C2), 2675–2692. https://doi.org/10.1029/90jc02422

Rintoul, S. R., & Trull, W. (2001). Water mass properties along a north-south hydrographic. *Journal of Geophysical Research*, *106*(C12), 31447–31462.

Robbins, L. L., & Brew, K. (1990). Proteins from the organic matrix of core-top and fossil planktonic foraminifera. *Geochimica Et Cosmochimica Acta*, *54*(8), 2285–2292. https://doi.org/10.1016/0016-7037(90)90052-M

Robinson, R. S., Kienast, M., Luiza Albuquerque, A., Altabet, M. A., Contreras, S., De Pol-Holz, R., … Yang, J. Y. (2012). A review of nitrogen isotopic alteration in marine sediments. *Paleoceanography*, *27*(PA4203), 1–13. https://doi.org/10.1029/2012PA002321

Robinson, R. S., Smart, S. M., Cybulski, J. D., McMahon, K. W., Marcks, B., & Nowakowski, C. (2023). Insights from Fossil-Bound Nitrogen Isotopes in Diatoms, Foraminifera, and Corals. *Annual Review of Marine Science*, *15*(1), 1–24. https://doi.org/10.1146/annurev-marine-032122-104001

Rohde, M. M., Granger, J., Sigman, D. M., & Lehmann, M. F. (2015). Coupled nitrate N and O stable isotope fractionation by a natural marine plankton consortium. *Frontiers in Marine Science*, *2*(May). https://doi.org/10.3389/fmars.2015.00028

Rühs, S., Durgadoo, J. V., Behrens, E., & Biastoch, A. (2013). Advective timescales and pathways of Agulhas leakage. *Geophysical Research Letters*, *40*, 3997–4000. https://doi.org/10.1002/grl.50782

Saino, T., & Hattori, A. (1980). ^{15}N natural abundance in oceanic suspended particulate matter. *Nature*, *283*, 752–754.

Salgueiro, E., Voelker, A. H. L., Martin, P. A., Rodrigues, T., Zúñiga, D., Froján, M., … Abrantes, F. (2020). δ^{18}O and Mg/Ca Thermometry in Planktonic Foraminifera: A Multiproxy Approach

Toward Tracing Coastal Upwelling Dynamics. *Paleoceanography and Paleoclimatology*, *35*(2), 1–27. https://doi.org/10.1029/2019PA003726

Samanta, S., Cloete, R., Dey, S., Barraqueta, J., Loock, J., Meynecke, J., de Bie, J., Vichi, M., Roychoudhury, A. (2023). Exchange of Pb from Indian to Atlantic Ocean Is Driven by Agulhas Current and Atmospheric Pb Input from South Africa. *Scientific Reports 13*(1), 5465. https://doi.org/10.1038/s41598-023-32613-5.

Sarmiento, J. L., Gruber, N., Brzezinski, M. A., & Dunne, J. P. (2004). High-latitude controls of thermocline nutrients and low latitude biological productivity. *Nature*, *427*(6969), 56–60. https://doi.org/10.1038/nature02127

Savoye, N., Aminot, A., Tréguer, P., Fontugne, M., Naulet, N., Kérouel, R. (2003). Dynamics of particulate organic matter $\delta^{15}N$ and $\delta^{13}C$ during spring phytoplankton blooms in a macrotidal ecosystem (Bay of Seine, France). *Marine Ecology Progress Series*, *255*, 27–41.

Schiebel, R., & Hemleben, C. (2005). Modern planktic foraminifera. *Paläontologische Zeitschrift*, *79*(1), 135–148. https://doi.org/10.1007/BF03021758

Schiebel, R., & Hemleben, C. (2017). *Planktic Foraminifers in the Modern Ocean* (1–358). Berlin: Springer-Verlag. https://doi.org/10.1007/978-3-662-50297-6

Schiebel, R., Smart, S. M., Jentzen, A., Jonkers, L., Morard, R., Meilland, J., … Haug, G. H. (2018). Advances in planktonic foraminifer research: New perspectives for paleoceanography. *Revue de Micropaleontologie*, *61*(3-4), 113–138. https://doi.org/10.1016/j.revmic.2018.10.001

Schmid, C., Boebel, O., Zenk, W., Lutjeharms, J. R. E., & Garzoli, S. L. (2003). Early evolution of an Agulhas Ring. *Deep Sea Research Part II*, *50*, 141–166.

Schmitt, R. W., & Olson, D. B. (1985). Wintertime convection in warm-core rings: Thermocline ventilation and the formation of mesoscale lenses. *Journal of Geophysical Research*, *90*(C5), 8823. https://doi.org/10.1029/jc090ic05p08823

Schouten, M., De Ruijter, W. P. M., Leeuwen, P. J. van, & Lutjeharms, J. R. E. (2000). Translation, decay and splitting of Agulhas rings in the southeastern Atlantic Ocean. *Journal of Geophysical Research*, *105*(9), 21913–21925.

Sen Gupta, B. K. (2003). *Modern Foraminifera* (Vol. 36, p. 384). https://doi.org/10.1007/0-306-48104-9

Siegel, D. A., Ohlmann, J. C., Washburn, L., Bidigare, R. R., Nosse, C. T., Fields, E., & Zhou, Y. (1995). Solar radiation, phytoplankton pigments and the radiant heating of the equatorial Pacific warm pool. *Journal of Geophysical Research*, *100*(C3), 4885–4891. https://doi.org/10.1029/94JC03128

Sigman, D. M., & Casciotti, K. L. (2009). Nitrogen Isotopes in the Ocean. *Encyclopedia of Ocean Sciences*, (Ms 632), 1884–1894. https://doi.org/10.1006/rwos.2001.0172

Sigman, D. M., Casciotti, K. L., Andreani, M., Barford, C., Galanter, M., & Böhlke, J. K. (2001). A bacterial method for the nitrogen isotopic analysis of nitrate in seawater and freshwater. *Analytical Chemistry*, *73*(17), 4145–4153. https://doi.org/10.1021/ac010088e

Sigman, D. M., DiFiore, P. J., Hain, M. P., Deutsch, C., Wang, Y., Karl, D. M., … Pantoja, S. (2009). The dual isotopes of deep nitrate as a constraint on the cycle and budget of oceanic fixed nitrogen. *Deep-Sea Research Part I: Oceanographic Research Papers*, *56*(9), 1419–1439. https://doi.org/10.1016/j.dsr.2009.04.007

Sigman, D. M., Granger, J., DiFiore, P. J., Lehmann, M. F., Ho, R., Cane, G., & Geen, A. van. (2005). Coupled nitrogen and oxygen isotope measurements of nitrate along the eastern North Pacific margin. *Global Biogeochemical Cycles*, *19*(4), 1–14. https://doi.org/10.1029/2005GB002458

Sigman, D. M., M. A, A., McCorkle, D. C., Francois, R., & Fischer, G. (1999). The δ15N of nitrate in the Southern Ocean: Nitrate consumption in surface waters. *Global Biogeochemical Cycles*, *13*(4), 1149–1166. https://doi.org/10.1029/1999GB900038

Simon, M. H., Ziegler, M., Barker, S., Meer, M. T. J. van der, Schouten, S., & Hall, I. R. (2020). A late Pleistocene dataset of Agulhas Current variability. *Scientific Data*, *7*(1), 1–12. https://doi.org/10.1038/s41597-020-00689-7

Sinha, A., Balwada, D., Tarshish, N., & Abernathey, R. (2019). Modulation of Lateral Transport by Submesoscale Flows and Inertia-Gravity Waves. *Journal of Advances in Modeling Earth Systems*, *11*(4), 1039–1065. https://doi.org/10.1029/2018MS001508

Smart, S. M., Fawcett, S. E., Ren, H., Schiebel, R., Tompkins, E. M., García, A. M., … Sigman, D. M. (2020). The Nitrogen Isotopic Composition of Tissue and Shell-Bound Organic Matter of Planktic Foraminifera in Southern Ocean Surface Waters. *Geochemistry, Geophysics, Geosystems*, *21*, 1–29.

Smart, S. M., Ren, H., Fawcett, S. E., Schiebel, R., Conte, M., Rafter, P. A., … Sigman, D. M. (2018). Ground-truthing the planktic foraminifer-bound nitrogen isotope paleo-proxy in the Sargasso Sea. *Geochimica Et Cosmochimica Acta*, *235*, 463–482. https://doi.org/10.1016/j.gca.2018.05.023

Sohm, J. A., Webb, E. A., & Capone, D. G. (2011). Emerging patterns of marine nitrogen fixation. *Nature Reviews Microbiology*, *9*(July), 499–508. https://doi.org/10.1038/nrmicro2594

Somes, C. J., Schmittner, A., Galbraith, E. D., Lehmann, M. F., Altabet, M. A., Montoya, J. P., … Eby, M. (2010). Simulating the global distribution of nitrogen isotopes in the ocean. *Global Biogeochemical Cycles*, *24*(4), 1–16. https://doi.org/10.1029/2009GB003767

Sousa, S. H. M., Godoi, S. S. de, Amaral, P. G. C., Vicente, T. M., Martins, M. V. A., Sorano, M. R. G. S., … Mahiques, M. M. (2014). Distribution of living planktonic foraminifera in relation to oceanic processes on the southeastern continental Brazilian margin (23 °S-25 °S and 40 °W-44 °W). *Continental Shelf Research*, *89*, 76–87. https://doi.org/10.1016/j.csr.2013.11.027

Spero, H. J., & Parker, S. L. (1985). Photosynthesis in the symbiotic planktonic foraminifer Orbulina universa, and its potential contribution to oceanic primary productivity. *Journal of Foraminiferal Research*, *15*(4), 273–281. https://doi.org/10.2113/gsjfr.15.4.273

Spero, H.J. (1988). Ultrastructural examination of chamber morphogenesis and biomineralization in the planktonic foraminifer *Orbulina universa*. *Marine Biology*, *99*(1), 9–20. https://doi.org/10.1007/BF00644972.

Spindler, M., Hemleben, C., Salomons, J. B., & Smit, L. P. (1984). Feeding behavior of some planktonic foraminifers in laboratory cultures. *Journal of Foraminiferal Research*, *14*(4), 237–249. https://doi.org/https://doi.org/10.2113/gsjfr.14.4.237

Stainbank, S., Kroon, D., Rüggeberg, A., Raddatz, J., Leau, E. S. de, Zhang, M., & Spezzaferri, S. (2019). Controls on planktonic foraminifera apparent calcification depths for the northern equatorial Indian Ocean. *PLoS One, 14(9),* e0222299. https://doi.org/10.1371/journal.pone.0222299

Steinhardt, J., De Nooijer, L. L. J., Brummer, G. J., & Reichart, G. J. (2015). Profiling planktonic foraminiferal crust formation. *Geochemistry, Geophysics, Geosystems*, *16*(7), 2409–2430. https://doi.org/10.1002/2015GC005752

Stramma, L., & Lutjeharms, J. R. E. (1997). The flow field of the subtropical gyre of the South Indian Ocean. *Journal of Geophysical Research*, *102*, 5513–5530.

Stramma, L., & Peterson, R. G. (1989). Geostrophic Transport in the Benguela Current Region. https://doi.org/10.1175/1520-0485(1989)019<1440:GTITBC>2.0.CO;2

Strickland, J. D. H., & Parsons, T. R. (1968). *A Practical Handbook of seawater analysis*. https://doi.org/10.2307/1979241

Treibergs, L. A., Fawcett, S. E., Lomas, M. W., & Sigman, D. M. (2014). Nitrogen isotopic response of prokaryotic and eukaryotic phytoplankton to nitrate availability in Sargasso Sea surface waters. *Limnology and Oceanography*, *59*(3), 972–985. https://doi.org/10.4319/lo.2014.59.3.0972

Tuerena, R. E., Ganeshram, R. S., Geibert, W., Fallick, A. E., Dougans, J., Tait, A., … Woodward, E. M. S. M. S. (2015). Nutrient cycling in the Atlantic basin: The evolution of nitrate isotope signatures in water masses. *Global Biogeochemical Cycles*, *29*, 1830–1844. https://doi.org/10.1002/2015GB005164.Received

Uhle, M. E., Macko, S. A., Spero, H. J., David W, L., Ruddiman, W. F., & Engel, M. H. (1999). The fate of nitrogen in the Orbulina universa foraminifera-symbiont system determined by nitrogen isotope analyses of shell-bound organic matter. *Limnology and Oceanography*, *44*(8), 1968–1977. https://doi.org/10.4319/lo.1999.44.8.1968

Uhle, M. E., Macko, S. A., Spero, H. J., Engel, M. H., & Lea, D. W. (1997). Sources of carbon and nitrogen in modern planktonic foraminifera: The role of algal symbionts as determined by bulk and compound specific stable isotopic analyses. *Organic Geochemistry*, *27*(3-4), 103–113. https://doi.org/10.1016/S0146-6380(97)00075-2

Van Aken, H. M., Van Veldhoven, A. K., Veth, C., De Ruijter, W. P. M., Van Leeuwen, P. J., Drijfhout, S. S., … Rouault, M. (2003). Observations of a young Agulhas ring, Astrid, during MARE in March 2000. *Deep-Sea Research Part II: Topical Studies in Oceanography*, *50*(1), 167–195. https://doi.org/10.1016/S0967-0645(02)00383-1

Van Oostende, N., Fawcett, S. E., Marconi, D., Lueders-Dumont, J., Sabadel, A. J. M., Woodward, E. M. S., … Ward, B. B. (2017). Variation of summer phytoplankton community composition and its relationship to nitrate and regenerated nitrogen assimilation across the North Atlantic Ocean. *Deep-Sea Research Part I: Oceanographic Research Papers*, *121*(June 2016), 79–94. https://doi.org/10.1016/j.dsr.2016.12.012

Wallschuss, S., Mdutyana, M., Parrott, R. G., Forrer, H. J., Roman, R., Walker, D., … Fawcett, S. E. (2022). The Influence of Agulhas Leakage on Primary Production and Nitrogen Cycling in the Southeastern Atlantic Ocean. *Journal of Geophysical Research: Oceans*, *127*, 1–26. https://doi.org/10.1029/2022JC018971

Wang, L., Huang, B., Laws, E. A., Zhou, K., Liu, X., Xie, Y., & Dai, M. (2018). Anticyclonic Eddy Edge Effects on Phytoplankton Communities and Particle Export in the Northern South China Sea. *Journal of Geophysical Research: Oceans*, *123*(11), 7632–7650. https://doi.org/10.1029/2017JC013623

Wankel, S. D., Kendall, C., Pennington, J. T., Chavez, F. P., & Paytan, A. (2007). Nitrification in the euphotic zone as evidenced by nitrate dual isotopic composition: Observations from Monterey Bay, California. *Global Biogeochemical Cycles*, *21*(2), 1–13. https://doi.org/10.1029/2006GB002723

Waterson, A. M., Edgar, K. M., Schmidt, D. N., & Valdes, P. J. (2017). Quantifying the stability of planktic foraminiferal physical niches between the Holocene and Last Glacial Maximum. *Paleoceanography*, *32*(1), 74–89. https://doi.org/10.1002/2016PA002964

Wefer, G., Berger, W. H., Siedler, G., & Werb, D. (1996). *The South Atlantic* (p. 644). Berlin Heidelberg: Springer.

Weigand, M. A., Foriel, J., Barnett, B., Oleynik, S., & Sigman, D. M. (2016). Updates to instrumentation and protocols for isotopic analysis of nitrate by the denitrifier method. *Rapid Communications in Mass Spectrometry*, *30*(12), 1365–1383. https://doi.org/10.1002/rcm.7570

Weijer, W., De Ruijter, W. P. M., Sterl, A., & Drijfhout, S. S. (2002). Response of the Atlantic overturning circulation to South Atlantic sources of buoyancy. *Global and Planetary Change*, *34*(3-4), 293–311. https://doi.org/10.1016/S0921-8181(02)00121-2

Whittle, C., Lutjeharms, J. R. E., Duncombe Rae, C. M., Shillington, F. A. (2008). Interaction of Agulhas filaments with mesoscale turbulence: a case study. *South African Journal of Science*, *104*, 135–139.

Wolff, E. W., Fischer, H., Fundel, F., Ruth, U., Twarloh, B., Littot, G. C., … Gaspari, V. (2006). Southern Ocean sea-ice extent, productivity and iron flux over the past eight glacial cycles. *Nature*, *440*(7083), 491–496. https://doi.org/10.1038/nature06271

Zarkogiannis, S., Kontakiotis, G., & Antonarakou, A. (2020). Recent planktonic foraminifera population and size response to Eastern Mediterranean hydrography. *Revue de Micropaleontologie*, *69*(100450), 1–10. https://doi.org/10.1016/j.revmic.2020.100450